POL-InSAR TRAINING COURSE

Shane R. CLOUDE

AEL Consultants
26 Westfield Avenue, Cupar, Fife, KY15 5AA
Scotland, UK
Tel/Fax : +44 1334 650761
e-mail : scloude@ieee.org, web : http://homepage.mac.com/aelc/

1   INTRODUCTION

In this course you will learn about a radar remote sensing technique called polarimetric interferometry [Cloude 1997,1998,2004, Papathanassiou 1998]. When used with an imaging synthetic aperture radar (SAR) system, it is usually termed Polarimetric Interferometric SAR or POLInSAR for short [Papathanassiou 2001]. POLInSAR has important applications in the remote measurement of vegetation properties such as forest height [Papathanassiou 2005] and biomass [Mette 2004] and developing future applications in agriculture [Williams 2005, Preiss 2005], snow/ice thickness monitoring [Dall 2003, Papathanssiou 2005] and urban height and structure applications [Schneider 2005]. As its name suggests, the technique combines two separate radar technologies, polarimetry and interferometry. The former involves switching the polarisation state of transmit and receive channels to measure differences in backscatter due to orientation, shape and material composition [Cloude 1996, Pottier 2005]. This leads ultimately to measurement of the 2x2 complex scattering matrix [S], from which we can synthesise the response of the image pixel to arbitrary polarisation combinations. Such radars are termed S-matrix or Quadpol systems (since four complex channels are measured by the radar, usually all possible combinations of horizontal and vertical linear polarisations HH, HV, VH and VV respectively)

On the other hand, radar interferometry [Bamler 1998] involves coherently combining signals from two separated spatial positions (defining the so called baseline of the interferometer) to extract a phase difference or interferogram. In radar this can be achieved in two main configurations, so called along-track interferometry, which involves time displacements between separated antennas along the flight direction of the platform leading to velocity estimation. Alternatively we can perform across-track interferometry, involving lateral separation of antennas and leading to spatial information relating to the elevation of the scatterer above a reference ground position. In POLInSAR interest centre mainly on across-track geometries but in principle it can be applied to along track configurations as well.

POLInSAR differs from conventional interferometry in that it allows generation of interferograms for arbitrary transmit/receive polarisation pairs. It turns out that the phase of an interferogram changes with the choice of polarisation and consequently we can extract important bio and geophysical parameters by interpreting this change in the right way. We shall see that consequently the combination of interferometry with polarimetry is greater than the sum of its parts and that POLInSAR allows us to overcome severe limitations of both techniques when taken alone. This is especially true in the important area of remote sensing of vegetated land surface, where polarimetry suffers from the inherent high entropy problem [Cloude 1996] while standard interferometry remains underdetermined i.e. the interferogram depends on many possible physical effects, no one of which can be identified from the data itself [Treuhaft 1996, 2000]. POLInSAR offers a window on a new way to overcome these limitations. In this course we develop the theory step by step, illustrating each stage with processed data and allowing the user to repeat the processing stages

The course begins with a review of the basis theory and notation before running through a 12 step practical training course covering most of the major steps involved in processing and analysis of POLInSAR data.

2 BACKGROUND THEORY

POLInSAR algorithms make use of signal coherence (or equivalently phase and local phase variance) rather than backscattered power [Zebker 1992, Hagberg 1995, Askne 1997, Touzi 1999]. For this reason we begin with a review of the techniques and problems associated with the estimation of coherence from radar data. We follow closely the approach developed in [Touzi 1999]. Starting with any two co-registered single look complex (SLC) data channels s_1 and s_2 the coherence is formally defined as shown in equation 1

$$\tilde{\gamma} = \gamma e^{i\phi} = \frac{E(s_1 s_2^*)}{\sqrt{E(s_1 s_1^*)} \cdot \sqrt{E(s_2 s_2^*)}} \qquad - 1)$$

where E(..) is the expected value and $0 \leq \gamma \leq 1$. In practice the sample coherence is frequently used as a coherence estimate of 1, as shown in equation 2

$$\tilde{\delta} = \delta e^{i\chi} = \frac{\sum_{i=1}^{L} s_{1i} s_{2i}^*}{\sqrt{\sum_{i=1}^{L} s_{1i} s_{1i}^*} \cdot \sqrt{\sum_{i=1}^{L} s_{2i} s_{2i}^*}} \qquad - 2)$$

where i is the sample number and we have only a finite number L independent signal measurements available. Equation 2 represents the maximum likelihood (ML) estimate of coherence and under some general statistical assumptions provides an estimate that is asymptotically unbiased. For jointly complex Gaussian processes (s_1, s_2) the probability density function (pdf) of δ can then be derived as a function of the true coherence value γ and the number of samples L as shown in 3 [Touzi 1999]

$$p(\delta|\gamma) = 2(L-1)(1-\gamma^2)^L \delta(1-\delta^2)^{L-2} F(L,L:1:\delta^2\gamma^2) \qquad - 3)$$

where F is a special mathematical function called the hypergeometric function [Touzi 1999]. More significant for POLInSAR is estimation of the bias in the coherence magnitude, derived from 3 as the first moment of δ and shown in equation 4

$$E(\delta) = \frac{\Gamma(L)\Gamma(1+\frac{1}{2})}{\Gamma(L+\frac{1}{2})} {}_3F_2(3/2,L,L;L+\frac{1}{2};1;\delta^2)(1-\delta^2)^L \qquad - 4)$$

where $_pF_q$ is the generalised hypergeometric function. The behaviour of this function can also be obtained through straightforward numerical simulation of Gaussian distributed signals (so avoiding the need to calculate $_pF_q$), shown for example in figure 1. Here we see that the estimate is consistently biased towards higher values (in the extreme case of 1–look estimation the coherence estimate is equal to unity and so always overestimated). However, importantly for us, the bias decreases with increasing number of independent samples L and with increasing underlying coherence γ.

A second important consequence of equation 3 is estimation of the variance of the sample coherence magnitude. This is required to assess the precision of parameters estimated from the coherence and impacts on the accuracy of derived products such as vegetation height. The most

accurate way to estimate this variance is as shown in equation 5. Note that the second term can be estimated from equation 3 while the first is shown in equation 6

$$\text{var}(\delta) = E(\delta^2) - E(\delta)^2 \qquad\qquad \text{var}(\delta) = E(\delta^2) - E(\delta)^2 \qquad\qquad - 5)$$

$$E(\delta^2) = \frac{\Gamma(L)\Gamma(1+1)}{\Gamma(L+1)} {}_3F_2(2,L,L;L+1;1;\delta^2)(1-\delta^2)^L \qquad - 6)$$

Similar considerations lead us to the following expression for the pdf of the corresponding interferometric phase, shown in 7

$$p(\chi \mid \phi,\gamma) = \frac{\Gamma(L+\tfrac{1}{2})(1-\gamma^2)^L\beta}{2\sqrt{\pi}\Gamma(L)(1-\beta^2)^{L+\frac{1}{2}}} + \frac{(1-\gamma^2)^L}{2\pi}F(L,1;\tfrac{1}{2};\beta^2) \ \text{ where } \begin{cases} -\pi < \chi \le \pi \\ \beta = \gamma\cos(\chi-\phi) \end{cases} \quad -7)$$

which can be used to formally estimate the variance of the phase estimate as shown in 8

$$\text{var}_\phi = \int_{-\pi}^{\pi} \chi^2 p(\chi \mid \phi,\gamma)d\chi \qquad\qquad - 8)$$

For a small number of looks, the hypergeometric functions can be replaced by simpler trigonometric functions [Lee 1994], but for L > 4, as generally required for POLInSAR applications, the full calculation is required. While these equations provide the most accurate method of assessing bias and complex coherence variance, often we assume zero bias (by using sufficient averaging) and estimate the variance by making use of simpler equations for speedier computation.

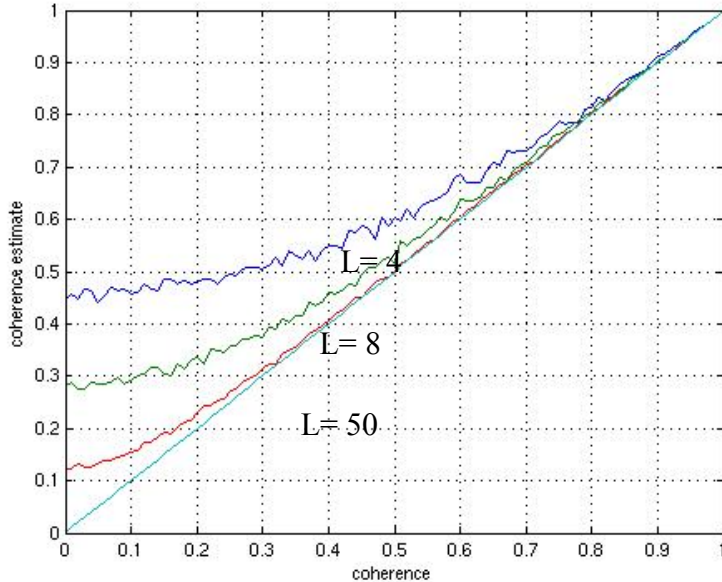*Figure 1: ML Coherence Bias as a function of coherence and number of looks*

In particular, the Cramer-Rao bounds provide lower limits on the variance for coherence and phase and have been derived in [Seymour 1994] to provide the simpler formulae shown in equation 9

$$\text{var}_\gamma = \frac{(1-\gamma^2)^2}{2L} \le \text{var}(\delta) \qquad \text{var}_\phi = \frac{1-\gamma^2}{2L\gamma^2} \le \text{var}(\chi) \qquad - 9)$$

In conclusion we note that for phase based processing, it is always better to operate at high coherence and avoid low coherences, the latter involving not only increased variance but also severe bias issues that can distort the phase information. It is a key limitation of polarimetry that scattering by vegetation leads to low coherences for all polarization channels (because of so called depolarization). This severely limits our ability to use polarimetric phase information over vegetated land surfaces. Interferometry on the other hand allows us to partially control coherence via baseline selection. POLInSAR exploits this advantage to obtain high coherence in multiple polarization channels.

The above considerations for coherence estimation are important in POLInSAR, the major distinguishing feature of which is that we add an extra stage in the construction of the two SLC channels s_1 and s_2. In general, for a QUADPOL data set, we take as input the three calibrated SLC images s_{hh}, s_{hv} and s_{vv} and generate projections of these onto user defined *complex* weight vectors $\underline{w}_1$ and $\underline{w}_2$ before calculating the coherence defined as shown in equation 10

$$
\left.
\begin{aligned}
s_1 &= w_1^1 \frac{(s_{hh}^1 + s_{vv}^1)}{\sqrt{2}} + w_1^2 \frac{(s_{hh}^1 - s_{vv}^1)}{\sqrt{2}} + w_1^3 \sqrt{2} s_{hv}^1 = \underline{w}_1^T . \underline{k}_1 \\
s_2 &= w_2^1 \frac{(s_{hh}^2 + s_{vv}^2)}{\sqrt{2}} + w_2^2 \frac{(s_{hh}^2 - s_{vv}^2)}{\sqrt{2}} + w_2^3 \sqrt{2} s_{hv}^2 = \underline{w}_2^T . \underline{k}_2
\end{aligned}
\right\}
\qquad \text{- 10)}
$$

$$
\Rightarrow \tilde{\gamma}(\underline{w}_1, \underline{w}_2) = \frac{E(s_1 s_2^*)}{\sqrt{E(s_1 s_1^*)} . \sqrt{E(s_2 s_2^*)}}
$$

The weight vectors $\underline{w}_1$ and $\underline{w}_2$ define user selected scattering mechanisms at ends 1 and 2 of the across-track baseline. In general $\underline{w}_1$ and $\underline{w}_2$ can be different and both parameterised as complex unitary vectors of the form shown in 11 [Cloude 1996, 1998]

$$
\underline{w} = \begin{bmatrix} w^1 & w^2 & w^3 \end{bmatrix} = \begin{bmatrix} \cos\alpha & \sin\alpha\cos\beta e^{i\varepsilon} & \sin\alpha\sin\beta e^{i\mu} \end{bmatrix}^T
\qquad \text{- 11)}
$$

Table I shows important examples of the weight vectors for coherence estimation in the commonly used linear, Pauli and circular bases. This table can be used together with equation 10 to generate interferograms in different polarisation channels. However, it is a feature of POLInSAR algorithm development that use is often made of more general $\underline{w}$ vectors than those shown, derived for example as eigenvectors for coherence optimisation [Cloude 1997, Tabb 2001,2002, Colin 2003, Gomez Dans 2005] or through a prior model studies of scattering from vegetated terrain [Williams 1999,2000]. For this reason we need to keep the more general notation of equation 11 so as to be able to consider arbitrary vectors in the formation of an interferogram. We now turn to consider such optimisation algorithms in more detail and to briefly assess their implications for coherence estimation and validation.

Polarisation Selection	α	β	ε	μ	1		
HH	45°	0°	0	0°	0.707	0.707	0
HV	90°	90°	0	0°	0	0	1
VV	45°	180°	0	0°	0.707	-0.707	0
HH+VV	0°	0°	0	0°	1	0	0
HH-VV	90°	0°	0	0°	0	1	0
LL	90°	45°	0	90°	0	0.707	0.707i
LR	0°	0°	0	0°	1	0	0
RR	90°	45°	0	-90°	0	0.707	-0.707i

Table I: Example scattering mechanisms used for POLInSAR

3   ALGORITHMS FOR OPTIMUM INTERFEROGRAM GENERATION

Polarimetric Interferometry is a special case of multi-channel coherent radar processing [Reigber 2000]. Such problems are characterised by multi-dimensional covariance matrices [Lee 1994, 1999, 2003]. In polarimetric SAR (POLSAR) for example, interest centres on the 3 x 3 hermitian coherency matrix [T], unitarily equivalent to the covariance matrix [C] as employed in multivariate statistical analyses [Lee 1999]. This is the basic building block in polarimetric interferometry and so we designate this matrix as Λ_1 to indicate how it relates to fully polarimetric measurements but made at only 1 spatial position. In single baseline POLInSAR we then add a second measurement at a displaced position 2. This is now characterised by a 6 x 6 coherency matrix Λ_2 as shown in equation 12. We see that this 6 x 6 matrix can be naturally partitioned into 3 sub matrices each of size 3 x 3. This formulation then scales in a natural way for multi-baseline POLInSAR by expansion of the governing coherency matrix Λ_N to a 3N x 3N complex system (4N x 4N for bistatic multi-baseline POLInSAR) as shown in 12

$$\Lambda_1 = [T] \rightarrow \Lambda_2 = \begin{bmatrix} T_1 & \Omega_{12} \\ \Omega_{12}^* & T_2 \end{bmatrix} \rightarrow \Lambda_N = \begin{vmatrix} T_1 & \Omega_{12} & \dots & \Omega_{1N} \\ \Omega_{12}^* & T_2 & \cdots & \Omega_{2N} \\ \vdots & \vdots & \ddots & \vdots \\ \Omega_{1N}^* & \Omega_{2N}^* & \cdots & T_N \end{vmatrix} \qquad \text{- 12)}$$

Returning now to the important case of Λ_2, two of the sub-matrices, T_1 and T_2 are Hermitian and relate to the polarimetry from positions 1 and 2 while the third Ω_{12} is a complex 3 x 3 matrix that contains information about the variation of interferometric coherence and phase for all possible weight vectors $\underline{w}_1$ and $\underline{w}_2$ as shown in equation 13.

$$\Lambda_2 = \begin{vmatrix} T_{11} & \Omega_{12} \\ \Omega_{12}^{*T} & T_{22} \end{vmatrix} \quad \Rightarrow \quad \tilde{\gamma}(\underline{w}_1, \underline{w}_2) = \frac{\underline{w}_1^{*T} \Omega_{12} \underline{w}_2}{\sqrt{\underline{w}_1^{*T} T_{11} \underline{w}_1} \cdot \sqrt{\underline{w}_2^{*T} T_{22} \underline{w}_2}} \qquad \text{- 13)}$$

This relation leads to an important choice of approach to algorithm development in POLInSAR. In the first case if we know the vectors $\underline{w}_1$ and $\underline{w}_2$ in advance, then we can directly estimate the coherence using equation 10 with the same InSAR fluctuation statistics and bias outlined in 4 and 8. However, often we wish to determine 'optimum' weight vectors from the data itself and it follows from 13 that to do this we require estimates of the three 3 x 3 matrices T_{11}, T_{22} and Ω_{12}. This opens up a much wider discussion about the fluctuation statistics and bias arising from the fact that only estimates and not true matrix values can be used in 13. For example, to estimate the submatrices we must first estimate the full 6 x 6 coherency matrix Λ_2. This estimate, Z, is obtained as a straightforward extension of equation 2 and is shown in 14, where we have L independent S-matrix (and hence scattering vectors $\underline{u}$) available [Lee 1999].

$$[Z] = \frac{1}{L} \sum_{j=1}^{L} \underline{u}_j \underline{u}_j^{*T} \qquad \text{- 14)}$$

For Gaussian statistics, this estimate [Z] of Λ follows a complex Wishart distribution [Lee 1999], so that its pdf is given for the general q dimensional case by equation 15

$$p_N([Z]|\Lambda) = \frac{L^L \det([Z])^{L-q} \exp(-L.Trace([\Lambda]^{-1}[Z]))}{K(L,q)\det([\Lambda])^L}$$ - 15)

$$K(L,q) = \pi^{0.5q(q-1)}\Gamma(L).\Gamma(L-q+1)$$

For interferometry we have seen q =2 leads to the statistics shown in 4 and 8. For S matrix polarimetry q = 3, while for single baseline POLInSAR q = 6. One key point to note is that the minimum number of data samples (L_{min}) required for adequate estimation of covariance matrices in multi-variate problems increases with the dimensionality q. Hence there are ever increasing demands on the number of looks required to obtain good estimates of derived products from multi-dimensional coherency matrix analysis.

One important application of this approach is the calculation of the optimum coherences in POLInSAR. The most general formulation of this was first presented in [Cloude 1997, 1998] and is summarised in equation 16. Here we first state the problem mathematically, which is to choose $\underline{w}_1$ and $\underline{w}_2$ so as to maximise the coherence magnitude, defined from the complex coherence as a function of the three sub-matrices T_{11} T_{22} and Ω_{12} as shown. This can be mathematically solved by using a Lagrange multiplier technique as shown and leads to the calculation of the required $\underline{w}$ vectors as eigenvectors of a pair of matrices, themselves defined as products of the composite matrices. Hence in order to calculate these we require first estimation of the 6x6 matrix Λ_2.

$$\max_{\underline{w}_1 \underline{w}_2} \frac{\underline{w}_1^{*T}\Omega_{12}\underline{w}_2}{\sqrt{\underline{w}_1^{*T}T_{11}\underline{w}_1.\underline{w}_2^{*T}T_{22}\underline{w}_2}}$$

$$L = \underline{w}_1^{*T}\Omega_{12}\underline{w}_1 + \lambda_1\left(\underline{w}_1^{*T}T_{11}\underline{w}_1 - 1\right) + \lambda_2\left(\underline{w}_2^{*T}T_{22}\underline{w}_2 - 1\right)$$ - 16)

$$\Rightarrow \begin{cases} \dfrac{\partial L}{\partial \underline{w}_1^{*T}} = \Omega_{12}\underline{w}_2 + \lambda_1 T_{11}\underline{w}_1 = 0 \\ \dfrac{\partial L}{\partial \underline{w}_2^{*T}} = \Omega_{12}^{*T}\underline{w}_1 + \lambda_2 T_{22}\underline{w}_2 = 0 \end{cases}$$

$$\Rightarrow \begin{cases} T_{22}^{-1}\Omega_{12}^{*T}T_{11}^{-1}\Omega_{12}\underline{w}_2 = \lambda_1\lambda_2^*\underline{w}_2 \\ T_{11}^{-1}\Omega_{12}T_{22}^{-1}\Omega_{12}^{*T}\underline{w}_1 = \lambda_1\lambda_2^*\underline{w}_1 \end{cases}$$

To illustrate the increased sample requirements we show a simple example based on numerical estimation of the eigenvalues and eigenvectors in equation 16 for an underlying coherency matrix Λ_2 of the form shown in 17

$$[\Lambda_2] = \begin{vmatrix} 1 & 0 & 0 & 0.9e^{i\frac{\pi}{4}} & 0 & 0 \\ 0 & 1 & 0 & 0 & 0.6e^{i\frac{\pi}{3}} & 0 \\ 0 & 0 & 1 & 0 & 0 & 0.4e^{i\frac{\pi}{2}} \\ 0.9e^{-i\frac{\pi}{4}} & 0 & 0 & 1 & 0 & 0 \\ 0 & 0.6e^{-i\frac{\pi}{3}} & 0 & 0 & 1 & 0 \\ 0 & 0 & 0.4e^{-i\frac{\pi}{2}} & 0 & 0 & 1 \end{vmatrix}$$ - 17)

which we see has a trivial solution with eigenvectors $\underline{w}_1 = \underline{w}_2$ equal to the basis vectors (1,0,0), (0,1,0) and (0,0,1) respectively and the optimum triplet of coherences are 0.9 0.6 and 0.4. If we now

use this matrix to generate complex Gaussian noise with the same underlying coherency matrix and use 16 to estimate the eigenvalues for varying number of looks then we obtain the results shown in figure 2. Here we plot the coherence estimates as a function of increasing number of looks. We show two sets of curves. In black we show the estimates based on a prior knowledge of the $\underline{w}$ vectors, using the projection and coherence estimation of equation 10. We see good convergence with the absence of any significant bias (each value on the curve is obtained as the mean of 256 realisations of the process so as to reduce the variance and hence expose any underlying bias issues). In the second case we show estimates based on the assumption of no a prior knowledge of the vectors i.e. when the vectors themselves must also be estimated from the raw data. Here we see a much slower convergence onto the true values with significant bias for a low number of looks. We see that the first 2 coherences are consistently overestimated while the third is underestimated. Only after a large number of looks does the bias reduce. For example for 10% coherence accuracy we require in excess of 40 looks, even for high coherence values. However, with care and sufficient averaging it has been shown that such optimisation can lead to better phase estimation for digital elevation model (DEM) generation [Nico 2000]
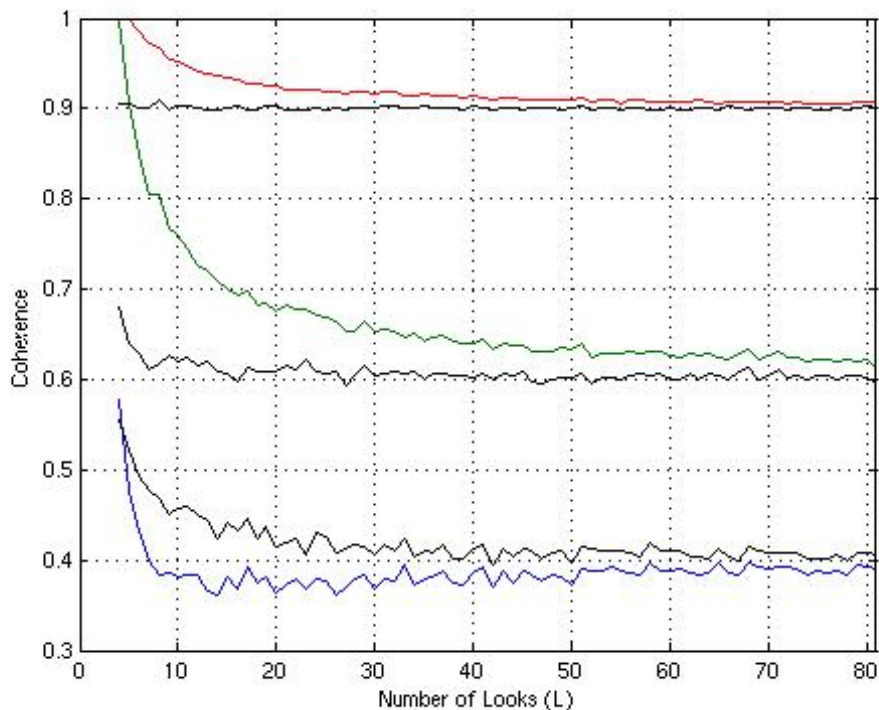

Figure 2 : Simulated Example of Optimum Coherence Estimation based on a prior knowledge of w vectors (black) and vectors derived from eigenvalue estimation (colour)

In order to obtain an optimization approach that has less bias for a given number of samples, it is necessary to reduce the effective dimensionality of the problem. Several authors have proposed adopting the a prior assumption that $\underline{w}_1 = \underline{w}_2$. i.e. that the optimum coherence vector remains unknown but we assume that it doesn't change with baseline [Sagues 2000, 2001, Flynn 2002, Pascual 2002, Colin 2003, Gomez Dans 2005]. This idea is supported on physical grounds for short baselines in the absence of temporal decorrelation i.e. for single pass or low frequency sensors where the scattering does not change significantly over the effective angular width of the baseline. This approach calls for a new mathematical formulation of the optimization process. One approach is based on a straightforward extension of the Lagrange multiplier technique to constrain $\underline{w}_1 = \underline{w}_2$

[Gomez Dans 2005]. This leads by manipulation of 16 to a set of $\underline{w}$ vectors given as eigenvectors of the composite matrix shown in 19

$$\left(T_{11} + T_{22}\right)^{-1}\left(\Omega_{12} + \Omega_{12}^{*T}\right)\underline{w} = -\lambda\underline{w} \qquad - 19)$$

One problem with 19 is that the eigenvalue is not the coherence, but its real part and so the optimization is phase sensitive. For this reason a second related approach based on maximization of the phase difference as a function of polarization vector $\underline{w}$. has been developed. In this case the optimum vector is found by solving a phase parameterised eigenvalue problem of the form shown in 20. [Flyn 2002, Colin 2003]

$$[\Omega_H]\underline{w} = \lambda[T]\underline{w} \qquad \begin{cases} [\Omega_H] = \dfrac{1}{2}\left(\Omega_{12}e^{i\phi_1} + \Omega_{12}^{*T}e^{-i\phi_1}\right) \\ [T] = \dfrac{1}{2}\left(T_{11} + T_{22}\right) \end{cases} \qquad -20)$$

This has been shown to be equivalent to calculating the numerical radius of the complex matrix $A = T^{-\frac{1}{2}}\Omega_{12}T^{-\frac{1}{2}}$. A proposed algorithm for finding this optimum state has been presented in [Colin 2003, 2005]. One drawback in this approach is that ϕ_1 is a free parameter and so either search or iterative methods must be used to secure the global optimum. This adds to the computational complexity for each pixel.

A third related approach has been proposed based on a sub-space Monte Carlo searching algorithm [Sagues 2000,2001]. This limits the search for the optimum (again assuming $\underline{w}_1 = \underline{w}_2$) to the diagonal elements of Ω_{12} i.e. to copolarised or crosspolarised combinations across the whole Poincaré sphere. This again acts to effectively limit the dimensionality of the problem and demonstrates less bias than the full Lagrange multiplier method. Finally, phase centre super-resolution techniques based on the ESPRIT algorithm have also been proposed to find the optimum $\underline{w}$ vectors. [Yamada 2001].

In all these cases a sub-optimum solution is obtained compared to the unconstrained Lagrange multiplier method but often with better numerical stability. Given the general increased processing overhead of employing optimization, it is of interest to investigate the potential benefits of employing an optimization approach over simple linear, Pauli and circular options (table I). To do this we look at a set of analytical solutions for the full optimizer.

In the previous section we formulated an important optimisation problem in POLInSAR, namely to investigate the maximum variation of coherence with polarisation by solving an eigenvalue problem. In this section we look at some canonical problems of interest in the remote sensing of land surfaces and try and use the mathematical solutions obtained to conclude as to the potential of optimisation versus standard coherence estimation in POLInSAR. We consider three important problems, scattering from non-vegetated surfaces, random volume scattering and finally a 2-layer surface+volume mixture which more closely matches the behaviour of natural vegetated land surfaces.

4   POLInSAR FOR BARE SURFACE SCATTERING

We start by considering the simplest case of non-vegetated terrain. Under the assumption of surface scattering only, the polarimetry can then be characterised as a reflection symmetric random media with a coherency matrix [T] of the form shown in equation 21 [Cloude 1996, 2004]. The

interferometry (following range spectral filtering [Gatelli 1994] and assuming no temporal or SNR decorrelation) is characterised by a single parameter, the ground phase ϕ as shown in 21.

$$K = T_{11}^{-1} \Omega_{12} T_{11}^{-1} \Omega_{12}^{*T}$$

- 21)

$$= \begin{bmatrix} t_{11} & t_{12} & 0 \\ t_{12}^* & t_{22} & 0 \\ 0 & 0 & t_{33} \end{bmatrix}^{-1} e^{i\phi} \begin{bmatrix} t_{11} & t_{12} & 0 \\ t_{12}^* & t_{22} & 0 \\ 0 & 0 & t_{33} \end{bmatrix} \begin{bmatrix} t_{11} & t_{12} & 0 \\ t_{12}^* & t_{22} & 0 \\ 0 & 0 & t_{33} \end{bmatrix}^{-1} e^{-i\phi} \begin{bmatrix} t_{11} & t_{12} & 0 \\ t_{12}^* & t_{22} & 0 \\ 0 & 0 & t_{33} \end{bmatrix} = \begin{bmatrix} 1 & 0 & 0 \\ 0 & 1 & 0 \\ 0 & 0 & 1 \end{bmatrix}$$

It follows from equation 16 that the optimum coherences are obtained as eigenvectors of the matrix [K] as shown. By multiplying terms we see that the matrix [K] is just the 3 x 3 identity matrix. This implies that all polarisations have the same interferometric coherence and POLInSAR plays no role in surface scattering problems. This is not quite true in practice for two important reasons: in practice there will be polarisation dependent SNR decorrelation. In fact, recently [Hajnsek 2005] it has been suggested that such SNR coherence variations with polarimetry be used for quantitative InSAR surface parameter estimation. This formulation assumes that the scattering from the surface occurs within a thin layer. If there is significant penetration into the surface then volume scattering effects can occur and this will lead to volume decorrelation effects (see below). These effects have been observed for land ice [Dall 2003] and snow studies [Papathanassiou 2005] where the surface is non-vegetated but covered by a low loss scattering layer. Nonetheless, equation 21 demonstrates how for bare surface scattering POLInSAR plays only a secondary role. More interesting for application of natural land surfaces is to consider the presence of volume scattering due to vegetation cover.

5   POLInSAR for Random Volume scattering

In case we consider scattering from a volume, interest centres on the special case of a random volume i.e. one with macroscopic azimuthal symmetry [Cloude 1996]. In this case the polarimetric coherency matrix [T] is diagonal. However more care is required over consideration of the interferometric phase in Ω_{12}. We now must include the effects of volume decorrelation due to the random vertical distribution of scatterers [Treuhaft 1996,2000, Cloude 2003]. In this case the interferometry must include a complex integral I_2 normalised by a real integral I_1 as shown in equation 22.

$$K = T_{11}^{-1} \Omega_{12} T_{11}^{-1} \Omega_{12}^{*T}$$

$$= \frac{1}{I_1} \begin{bmatrix} \frac{1}{t_{11}} & 0 & 0 \\ 0 & \frac{1}{t_{22}} & 0 \\ 0 & 0 & \frac{1}{t_{33}} \end{bmatrix} I_2 \begin{bmatrix} t_{11} & 0 & 0 \\ 0 & t_{22} & 0 \\ 0 & 0 & t_{33} \end{bmatrix} \frac{1}{I_1} \begin{bmatrix} \frac{1}{t_{11}} & 0 & 0 \\ 0 & \frac{1}{t_{22}} & 0 \\ 0 & 0 & \frac{1}{t_{33}} \end{bmatrix} I_2^* \begin{bmatrix} t_{11} & 0 & 0 \\ 0 & t_{22} & 0 \\ 0 & 0 & t_{33} \end{bmatrix}$$

- 22)

$$= \left| \frac{I_2}{I_1} \right|^2 \begin{bmatrix} 1 & 0 & 0 \\ 0 & 1 & 0 \\ 0 & 0 & 1 \end{bmatrix}$$

Here we again see that [K] is proportional to the identity matrix but this time the eigenvalues (all equal) are given by a ratio of integrals over the vertical distribution. This ratio is just the volume

decorrelation displaying an increase in phase variance and a vegetation bias to the ground phase determined by two parameters, namely the height of the vegetation and its mean extinction coefficient σ as shown in equation 23. Here the vertical interferometric wavenumber k_z [Bamler 1998] appears as a function of the baseline to wavelength ratio B/λ as well as the sensor height H and angle of incidence θ.

$$\tilde{\gamma}(\underline{w}) = \frac{I_2}{I_1} = \frac{e^{-\frac{2\sigma h_v}{\cos\theta_o}} \int_0^h e^{\frac{2\sigma z'}{\cos\theta_o}} e^{ik_z z'} dz'}{e^{-\frac{2\sigma h_v}{\cos\theta_o}} \int_0^h e^{\frac{2\sigma z'}{\cos\theta_o}} dz'} = \frac{2\sigma e^{i\phi(z_o)}}{\cos\theta_o (e^{2\sigma h_v/\cos\theta_o} - 1)} \int_0^h e^{ik_z z'} e^{\frac{2\sigma z'}{\cos\theta_o}} dz'$$

$$= \frac{p}{p_1} \frac{e^{p_1 h_v} - 1}{e^{p h_v} - 1} \text{ where } \begin{cases} p = \dfrac{2\sigma}{\cos\theta} \\ p_1 = p + ik_z \qquad = \tilde{\gamma}_v \\ k_z = \dfrac{4\pi\Delta\theta}{\lambda\sin\theta} \approx \dfrac{4\pi B_n}{\lambda H \tan\theta} \end{cases}$$

$$- 23)$$

where Δθ is the angular separation of the baseline end points from the surface pixel. Note that the vegetation is characterized by a height h_v and mean extinction rate σ as shown, both parameters of interest in remote sensing. Again however we note that this coherence is independent of polarisation, [K] has 3 degenerate eigenvalues and POLInSAR plays no role in the analysis of random volume scattering. This statement has to be modified in the presence of oriented volumes [Treuhaft 1999, Cloude 2000] i.e. ones with a preferred orientation of scattering elements such as occur in some agricultural crops and even in forestry applications at low frequencies [Cloude 2000]. In such cases POLInSAR does indeed play a role for volume scattering, with [K] developing 3 distinct eigenvalues. However for the treatment of forestry applications at L band and above such orientation effects are small and the random volume assumption is justified [Papathanssiou 1999, 2000].

In conclusion, both bare surfaces and random volumes lead to a degenerate eigenvalue spectrum for the matrix [K]. It is only when we combine these two effects together that we start to see the potential benefits of employing POLInSAR processing.

6   POLInSAR : 2-LAYER COMBINED SURFACE AND RANDOM VOLUME SCATTERING

In the general case when combined surface and volume scattering occurs then POLInSAR coherence optimisation becomes useful as we now demonstrate. In this 2-layer case or random-volume-over-ground (rvog) model approach [Treuhaft 2000, Cloude 2003], the observed coherence is given by a mixture formula as shown in 24. Here the ground phase ϕ and complex volume coherence $\tilde{\gamma}_v$ are combined with a new real parameter μ, the ratio of effective surface (i.e. all scattering contributions with a phase centre located at ϕ) to volume scattering. In effect when μ = 0 we resort to the case of random volume scattering while when μ tends to infinity then we resort to the surface scattering case. Interest centres on the intermediate case because here we have an unknown but constant complex number contribution from the volume scattering combined with a polarisation dependent surface term. By isolating the polarisation dependent terms the resulting coherence then lies along a straight line in the complex coherence plane as shown in 24.

$$\tilde{\gamma}(\underline{w}) = e^{i\phi}\frac{\tilde{\gamma}_v + \mu(\underline{w})}{1 + \mu(\underline{w})} = e^{i\phi}[\tilde{\gamma}_v + \frac{\mu(\underline{w})}{1 + \mu(\underline{w})}(1 - \tilde{\gamma}_v)] \qquad - 24)$$

This straight line model has been successfully tested on varied forest data sets [Isola 2001, Papathanassiou 2001, 2005] and seems to be a good fit for L and P band POLInSAR forestry applications. It is interesting to note how the coherence varies as we adjust the single parameter μ along this line. Figure 3 illustrates three important cases. In all three we first note how the coherence starts for small μ at some value depending on the volume scattering contribution (0.8 in the example). It then initially *decreases* with increasing surface contribution until reaching a turning point after which it *increases* with μ, always approaching unity as μ tends to infinity.

In figure 3 we superimpose three important special cases of the eigenvalue spectrum of [K] for this scenario. In the top we show the case when μ is always small (i.e. when there is strong volume scattering with high extinction masking the surface contributions). Here we see that as we adjust polarisation (<u>w</u>) then μ will also change and the optimiser has an incentive to select the *minimum* μ channel to *maximise* coherence. At the other extreme, when μ is large and surface scattering dominates, we see that the optimiser has an incentive instead to *maximise* μ in order to *maximise* coherence. A more interesting case (and one that occurs often in practice for L band forestry applications) is the intermediate zone when the variation of μ (the μ spectrum) includes the turning point. In this case the coherence can be maximised by either increasing or decreasing μ depending on circumstances.

We make two important conclusions from this, firstly that in the mixed surface + volume scattering case the coherence varies with polarisation and so optimisation plays a role in POLInSAR analysis. Secondly we see that we cannot simply associate the maximum coherence with for example the maximum value of μ. Both maxima and minima of μ can lead to the optimum coherence, depending on the circumstances. However it follows that if we can estimate the μ spectrum for any problem then we can compare the max/min with the values for the standard channel (linear, Pauli etc) to quantify the potential benefits of employing optimisation techniques.

Determination of the extreme points of the μ spectrum is related to a classical problem in radar polarimetry, namely contrast optimisation [Novak 1990]. The solution to this is obtained as the eigenvalues of the product of the inverse volume times the surface polarimetric coherency matrices as shown in 25.

$$T_V = mI_1\begin{bmatrix} 1 & 0 & 0 \\ 0 & \kappa & 0 \\ 0 & 0 & \kappa \end{bmatrix} \Rightarrow T_v^{-1} = \frac{1}{mI_1}\begin{bmatrix} 1 & 0 & 0 \\ 0 & \frac{1}{\kappa} & 0 \\ 0 & 0 & \frac{1}{\kappa} \end{bmatrix} \Rightarrow T_v^{-1}T_s = \frac{1}{I_1m}\begin{bmatrix} t_{11} & t_{12} & 0 \\ \frac{t_{12}^*}{\kappa} & \frac{t_{22}}{\kappa} & 0 \\ 0 & 0 & \frac{t_{33}}{\kappa} \end{bmatrix} \qquad - 25)$$

$$T_s = \begin{bmatrix} t_{11} & t_{12} & 0 \\ t_{12}^* & t_{22} & 0 \\ 0 & 0 & t_{33} \end{bmatrix}$$

Under the assumption of a random volume and reflection symmetric surface scattering component, the eigenvalues of this matrix can be determined analytically as shown in equation 26.

$$
\begin{cases}
\mu_1 = \dfrac{1}{2I_1 m}\left(t_{11} + \dfrac{t_{22}}{\kappa} + \sqrt{\left(t_{11} - \dfrac{t_{22}}{\kappa} \right)^2 + \dfrac{4|t_{12}|^2}{\kappa}} \right) \\[4mm]
\mu_2 = \dfrac{1}{2I_1 m}\left(t_{11} + \dfrac{t_{22}}{\kappa} - \sqrt{\left(t_{11} - \dfrac{t_{22}}{\kappa} \right)^2 + \dfrac{4|t_{12}|^2}{\kappa}} \right) \\[4mm]
\mu_3 = \dfrac{1}{I_1 m}\left(\dfrac{t_{33}}{\kappa} \right)
\end{cases}
\Rightarrow
\begin{cases}
\gamma_1 e^{i\delta_1} = \dfrac{e^{i\phi_o}(\gamma_v + \mu_1)}{1 + \mu_1} \\[4mm]
\gamma_2 e^{i\delta_2} = \dfrac{e^{i\phi_o}(\gamma_v + \mu_2)}{1 + \mu_2} \\[4mm]
\gamma_3 e^{i\delta_3} = \dfrac{e^{i\phi_o}(\gamma_v + \mu_3)}{1 + \mu_3}
\end{cases}
\qquad \text{- 26)}
$$

Equally importantly, the eigenvectors of this matrix indicate the <u>w</u> vectors that should be employed in POLInSAR to secure these extreme coherence values. We note from 26 that the optimum contrast solutions are not generally the simple HH, HV and VV channels and this supports investigation of optimisation techniques based on full quadpol data acquisition for POLInSAR Processing.
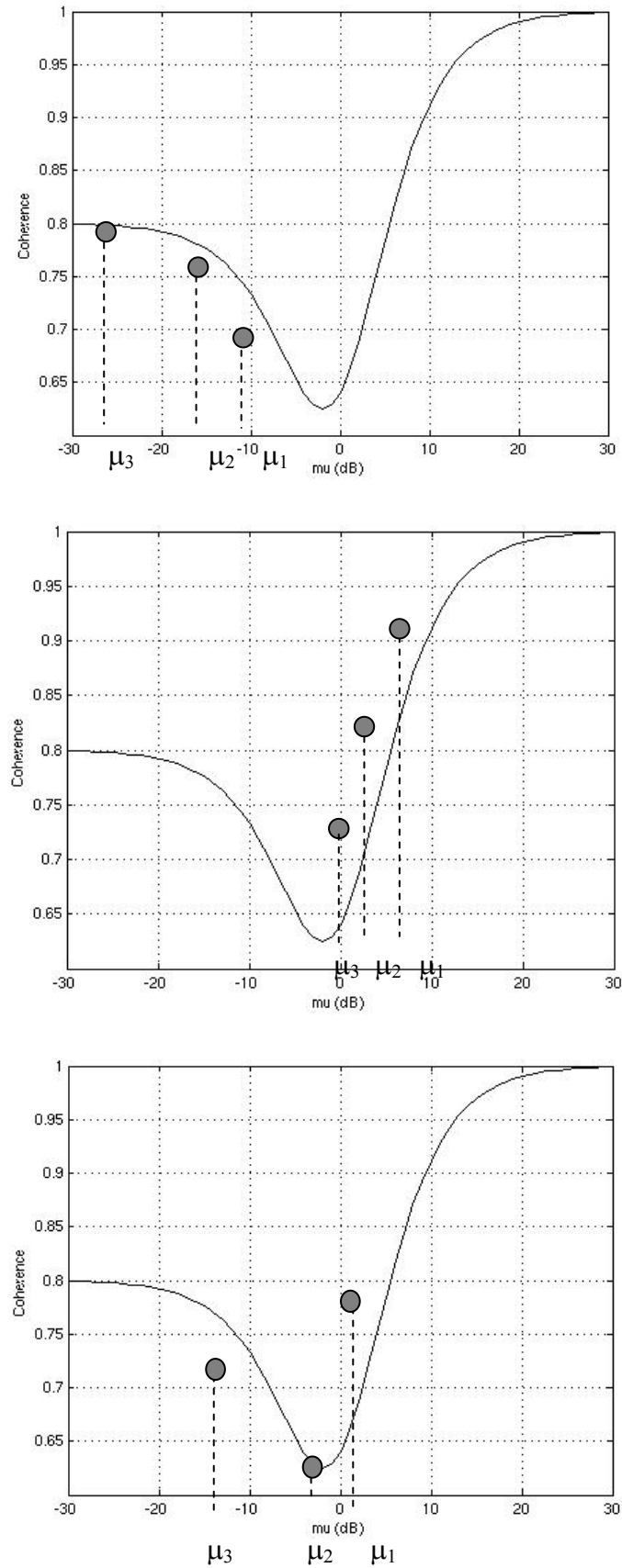
Figure 3 : Variation of Coherence with small (top), large(centre) and intermediate (lower) μ values

7   ALGORITHMS FOR VEGETATION PARAMETER RETRIEVAL

We have seen in equation 26 that the coherence of vegetated land surfaces depends on several important vegetation and surface parameters. The two most important of these are the mean vegetation height and the true ground topographic phase. These two are important products for scientific and commercial applications in their own right but also offer the possibility of estimating important secondary products such as vegetation biomass [Mette 2004]. Here we summarise the main algorithms used for generation of vegetation height and ground topography products from single baseline POLInSAR.

In general, we obtain POLInSAR products by employing model based parameter estimation, whereby using a scattering model M with parameters $\underline{p}$ we make observations of a set $\underline{o}$ and then obtain estimates of the parameters by inverting the model so that formally we can write

$$\underline{p} = M^{-1}\underline{o}$$

- 27)

where the inverse is often approximated by using a least squares approach so that the parameters are chosen so as to minimise the difference between the observations and the model predictions. In our case M is of the form given by the 'rvog' 2-layer coherence model so that we can formulate 27 as shown in equation 28

$$\left. \begin{array}{l} \gamma_1 e^{i\delta_1} = \dfrac{e^{i\phi_o}\left(\gamma(h_v,\sigma)+\mu_1\right)}{1+\mu_1} = f_1(\phi_o,h_v,\sigma) \\[2mm] \gamma_2 e^{i\delta_2} = \dfrac{e^{i\phi_o}\left(\gamma(h_v,\sigma)+\mu_2\right)}{1+\mu_2} = f_2(\phi_o,h_v,\sigma) \\[2mm] \gamma_3 e^{i\delta 3} = \dfrac{e^{i\phi_o}\left(\gamma(h_v,\sigma)+\mu_3\right)}{1+\mu_3} = f_3(\phi_o,h_v,\sigma) \end{array} \right\} \Rightarrow \underline{p} = \begin{pmatrix} \phi_o \\ h_v \\ \sigma \\ \mu_1 \\ \mu_2 \\ \mu_3 \end{pmatrix}, \underline{o} = \begin{pmatrix} \tilde{\gamma}_1 \\ \tilde{\gamma}_2 \\ \tilde{\gamma}_3 \end{pmatrix}$$

- 28)

Note that we have 6 parameters and 6 observations (3 complex coherences). It is clear also that we should choose the three coherence values to be as different as possible so as to maximise stability of the inversion. This can be achieved either through physical knowledge of the problem (e.g. using HV for the volume channel and HH for a surface dominated channel) or via use of an appropriate optimizer as discussed in equation 26. Of particular importance as products are the first two elements of $\underline{p}$, namely ground topography and mean vegetation height, although the m estimates have recently been proposed for foliage penetration [Cloude 2004] and surface parameter estimation [Cloude 2005]. We can obtain estimates of these (i.e. invert M) via various inversion strategies as we now show.

To start we need to estimate the phase ϕ_o. There are two basic ways to do this. The first is to select a polarisation channel via choice of a weight vector $\underline{w}_s$ where it is assumed μ is very large. At P-band for example HH is often employed [Cloude 2000]. At L band HH can again be used or HH-VV if Quadpol data is available. In this case $\hat{\phi}$ the estimate of ϕ_o is then simply obtained as

$$\hat{\phi} = \arg(\tilde{\gamma}_{\underline{w}_s})$$

- 29)

The problem here is to find the best polarisation $\underline{w}_S$. Extensive analysis of L and P band data sets have shown that in general there is no single $\underline{w}_S$ that yields an unbiased estimate of ϕ_o. For this

reason a second class of algorithms have been developed where we attempt residual bias removal using the 'rvog' model by employing a pair of complex coherence values as follows.

As equation 28 represents a straight line in the complex plane it follows that one simple algorithm is to employ a straight line fit to a pair of coherence values at polarisations $\underline{w}_S$ and $\underline{w}_V$, where the latter is volume dominated and the former surface dominated. The intersection of this line with the unit circle of the complex coherence plane yields 2 candidate points for the ground phase. To resolve the ambiguity between these two points, it must be assumed in advance that the $\underline{w}_S$ combination has a phase centre closer to the ground than $\underline{w}_V$ In this case we can solve for ϕ_o by using the first two equations (for γ_1 and γ_2) in 28 and setting $\mu_1 = 0$. This leads to a quadratic equation as shown in 30. In a more general approach, coherences for 3 or more polarisation combinations ($\underline{w}$ vectors) can be combined to yield an over-determined least squares estimate of the line fit. Either a simple standard least squares fit between the real and imaginary or a total least squares fit to the 2-D problem can be employed. This LS line is then used to find the 2 intersection points with the unit circle and again the ambiguity is resolved by allocating a rank ordering to the coherence values. Usually it is assumed that HV is higher in the canopy than HH and this can be used to resolve the ambiguity. Note however that for a small number of looks and low coherences such a strategy may be noisy (see figure 21).

$$\hat{\phi} = \arg(\tilde{\gamma}_{\underline{w}_V} - \tilde{\gamma}_{\underline{w}_S}(1 - L_{\underline{w}_S})) \quad 0 \le L_{\underline{w}_S} \le 1$$

$$AL_{\underline{w}_S}^2 + BL_{\underline{w}_S} + C = 0 \Rightarrow L_{\underline{w}_S} = \frac{-B - \sqrt{B^2 - 4AC}}{2A} \tag{- 30}$$

$$A = |\tilde{\gamma}_{\underline{w}_S}|^2 - 1 \quad B = 2\operatorname{Re}((\tilde{\gamma}_{\underline{w}_V} - \tilde{\gamma}_{\underline{w}_S}).\tilde{\gamma}_{\underline{w}_S}^*) \quad C = |\tilde{\gamma}_{\underline{w}_V} - \tilde{\gamma}_{\underline{w}_S}|^2$$

Having obtained an estimate of the ground phase ϕ_o. the second stage is then to estimate the height

8   FOREST HEIGHT INVERSION ALGORITHM
There are 3 main approaches used to estimate vegetation height from POLInSAR data:

8.1   DEM DIFFERENCING

In this approach we employ the same idea as used in the estimation of the ground phase to isolate a polarisation channel that scatters from the top of the canopy and hence generate a height estimate directly as shown in equation 31

$$h_v = \frac{\arg(\gamma_{\underline{w}_V}) - \hat{\phi}}{k_z}, \quad k_z = \frac{4\pi\Delta\theta}{\lambda\sin\theta} \approx \frac{4\pi B_n}{\lambda R\sin\theta} \tag{- 31}$$

where $\underline{w}_V$ is a user selected polarisation, assumed to be located at the top of the vegetation. Often this is taken to be HV, as this channel is dominated by volume scattering. Alternatively, phase optimisation based on the ESPRIT algorithm [Yamada 2001] or numerical radius estimation [Colin 2005] can be used. Note however that HV phase centre can lie anywhere between half the tree height and the top of the canopy itself. The exact location depends on two properties of the vegetation, namely the mean wave extinction and vertical canopy structure variation. In case the trees have a high thin canopy then extinction is small but the phase centre is high due to the structure. On the other hand, when the canopy extends over the full tree height then the phase centre can be at half the true height for low density (small extinction) through to the top of the canopy for

dense vegetation (high extinction). This ambiguity is inherent to single baseline methods and to combat this we need to employ model based correction methods as we now consider.

8.2   HEIGHT COMPENSATED FOR EXTINCTION

In this approach we use the extinction variation to compensate both density and structure variations but obtain a reliable estimate of height [Cloude 2002, Papathanassiou 2001]. In this way we sacrifice accuracy of retrieval of extinction for robustness in the height parameter. To do this we use the algorithm shown in 32. Here we make use of the previously estimated ground phase and the full 'rvog' model to match the model against observation of a coherence in a channel $\gamma(\underline{w})$, which we expect to be volume dominated. However, in doing so we have no idea of the surface-to-volume scattering ratio in that channel. Consequently there are an infinity of possible candidate 'volume-only' points along the line. These are parameterised by the parameter $0 \le \lambda \le 1$ in equation 32. If $\lambda = 0$ then we assume that $\gamma(\underline{w})$ is the volume only coherence itself ($\mu = 0$). At the other extreme the volume-only point can lie on the unit circle at the far end of the coherence line with phase ϕ_2 as shown in 32.

$$\min_{h_v,\sigma} L_1(\lambda,\underline{w}) = \left\| \tilde{\gamma}(\underline{w}) + \lambda\left(e^{i\hat{\phi}_2} - \tilde{\gamma}(\underline{w})\right) - e^{i\hat{\phi}} \frac{p}{p_1} \frac{e^{p_1 h_v}-1}{e^{ph_v}-1} \right\|$$

$$\text{where} \begin{cases} p = \dfrac{2\sigma}{\cos\theta} \\ p_1 = p + ik_z \\ \hat{\phi}_2 = \arg(\tilde{\gamma}_{\underline{w}_V} - \tilde{\gamma}_{\underline{w}_S}\left(1 - L_{\underline{w}_V}\right)) \end{cases}, k_z = \frac{4\pi\Delta\theta}{\lambda\sin\theta} \approx \frac{4\pi B_n}{\lambda R\sin\theta} \qquad - 32)$$

In order to resolve these multiple solutions the user must select a value of λ. The usual choice is to set $\lambda = 0$ by assuming that $\underline{w} = \underline{w}_V$ corresponds to a state with $\mu = 0$ (HV for example), in which case inversion simplifies as shown in 33.

$$\min_{h_v,\sigma} L_1(\lambda=0) = \left\| \tilde{\gamma}_{\underline{w}_V} - e^{i\hat{\phi}} \frac{p}{p_1} \frac{e^{p_1 h_v}-1}{e^{ph_v}-1} \right\| \text{ where} \begin{cases} p = \dfrac{2\sigma}{\cos\theta} \\ p_1 = p + ik_z \end{cases} \qquad - 33)$$

In this expression k_z and θ are known from the radar geometry and there are 2 unknowns, h_v and σ. As stated above, the parameter σ absorbs variations in density and structure of the vegetation and hence tends to be noisy. Equation 33 can be applied to invert real data in one of 2 ways, either by iterative search methods (such as the simplex method), starting with an initial guess and then converging on the minimum norm solution, or by use of look up tables (LUT). In the latter case the range of extinction values used in the LUT should be extended to accommodate variations of structure as well as expected extinction rates for the radar centre frequency. Failure to do this can lead to LUT boundary effects causing apparent saturation of the estimate. A way to overcome this LUT limitation will be presented in equation 37. Note that since the coherence and phase are both required to obtain a solution, then this approach is sensitive to calibration errors, especially in coherence [Cloude 2002]. However this approach has demonstrated, for airborne and chamber based data, the best height retrieval accuracy of all POLInSAR algorithms to date [Mette 2004, Papathanassiou 2005, Sagues 2000].

8.3 HEIGHT COMPENSATED FOR VERTICAL STRUCTURE

As an alternative strategy we can fix the extinction at some mean value $\overline{\sigma}$ appropriate for the radar frequency and then ascribe all variations in volume coherence to vertical structure. One way to do this is to use empirical extinction relationships published in the literature and derived from a mean of airborne measurements on different forest types [Bessette 2001]. This leads to a relation of the form shown in equation 34, where A is the 2-way total extinction (in dB), θ the angle of incidence, f the frequency in MHz and α and β regression coefficients. These are shown in table II for H and V polarisations. Note that these relationships are derived for low frequency operation (valid for L band and below). We see that in fact there is a slight differential extinction with VV having a higher extinction than HH. However the effect is small and in practice we can ignore this and take the mean extinction for input to the 'rvog' model.

$$A\cos\theta = \alpha . f^{\beta} \qquad - 34)$$

Attenuation factors		
HH	0.18	0.53
VV	0.3	0.47

Table II :Mean Extinction Regression Parameters

Relations such as this, or more direct EM modelling of propagation extinction in random media [Williams 2000], can be used to estimate the mean extinction rate in dB/m for an estimated canopy thickness. The simplest way to then model variations in vertical structure is to allow for an offset canopy from the reference ground phase [Cloude 2001,2002]. In this way height estimation is augmented by a second parameter, canopy thickness d ($0 \le d \le h_v$) in a modified 'rvog' model inversion as shown in 35.

$$\min_{h_v,d} L_1(\lambda = 0) = \left\| \tilde{\gamma}_{\underline{w}_v} - e^{i\hat{\phi}} e^{ik_z(h_v-d)} \frac{p}{p_1} \frac{e^{p_1 d}-1}{e^{pd}-1} \right\| \text{ where} \begin{cases} p = \dfrac{2\overline{\sigma}}{\cos\theta} \\ p_1 = p + ik_z \end{cases} \qquad - 35)$$

This model has been applied to height retrieval for tree species with high thin canopies such as mature Scots Pine in the Glen Affric region of Scotland [Cloude 2001].

8.4 HEIGHT FROM COHERENCE AMPLITUDE ONLY

In the discussion around equation 30, we highlighted one potential problem with ground phase estimation in low coherence regions, namely that in come circumstances it can be difficult to resolve the ambiguity between the two intersection points on the unit circle. In these cases, two height solutions can be found for the same point. To avoid errors of this type we can isolate such points by checking solutions for both intersection points and flagging those that suggest ambiguous height solutions. However we then need to employ an alternative height estimation algorithm on these points. One possible technique is to ignore the phase of the coherence completely and to select a polarisation channel with expected low surface to volume scattering ratio (HV for example). The coherence *amplitude* in this channel is then compared with the random volume prediction to obtain a height estimate. One limitation of this method is that the estimate remains sensitive to density and vertical structure variations. Two main options are available, in the first the extinction is set to zero and we obtain the simple 'sinc' coherence model. In the second we can employ a mean extinction as in table II. In any case, the height estimate is then obtained as a solution of the following equation:

$$\min_{h_v} L_1 = \left\| \left| \tilde{\gamma}_{\underline{w}_v} \right| - \left| \frac{p}{p_1} \frac{e^{p_1 h_v} - 1}{e^{p h_v} - 1} \right| \right\| \text{ where } \begin{cases} p = \dfrac{2\bar{\sigma}}{\cos\theta} \\[2mm] p_1 = p + ik_z, k_z = \dfrac{4\pi\Delta\theta}{\lambda\sin\theta} \approx \dfrac{4\pi B_n}{\lambda R\sin\theta} \end{cases}$$ - 36)

As it ignores phase and is sensitive to extinction and structure variations, this method is the least robust of the algorithms, but as stated above its main role has been as a back up solution when other approaches fail.

8.5   ROBUST INVERSION ACCOUNTING FOR EXTINCTION/VERTICAL STRUCTURE

We can use the above observations to develop a hybrid approach based on fusion of the coherence amplitude and DEM differencing algorithm. This algorithm is much faster and easier to implement than the full 'rvog' inversion (equation 32) and yet is also robust to variations in extinction or vertical structure as we now demonstrate. Although based on an approximation, this algorithm nonetheless gives height estimates within 10% accuracy, matching the bounds achievable with current air and space borne sensors [Papathanassiou 2005].

The algorithm requires selection of two interferograms, one for a surface *dominated* channel $\underline{w}_s$ and the second for a volume *dominated* channel $\underline{w}_v$. The forest height can then be estimated as shown in equation 37

$$h_v = \frac{\arg(\tilde{\gamma}_{\underline{w}_v}) - \hat{\phi}}{k_z} + \varepsilon \frac{2\sin c^{-1}(|\tilde{\gamma}_{\underline{w}_v}|)}{k_z}$$

where

$$\hat{\phi} = \arg(\tilde{\gamma}_{\underline{w}_v} - \tilde{\gamma}_{\underline{w}_s}(1 - L_{\underline{w}_s})) \quad 0 \le L_{\underline{w}_s} \le 1$$ - 37)

$$AL_{\underline{w}_s}^2 + BL_{\underline{w}_s} + C = 0 \Rightarrow L_{\underline{w}_s} = \frac{-B - \sqrt{B^2 - 4AC}}{2A}$$

$$A = \left|\tilde{\gamma}_{\underline{w}_s}\right|^2 - 1 \quad B = 2\operatorname{Re}((\tilde{\gamma}_{\underline{w}_v} - \tilde{\gamma}_{\underline{w}_s}).\tilde{\gamma}_{\underline{w}_s}^*) \quad C = \left|\tilde{\gamma}_{\underline{w}_v} - \tilde{\gamma}_{\underline{w}_s}\right|^2$$

We see that the height is obtained as a sum of 2 components. The first is just the height from phase or DEM difference between the estimated ground topography point and estimated volume only complex coherence. Importantly, unlike the case in equation 31, this polarisation need not be at the top of the vegetation and to compensate this, the height estimate is augmented by the second coherence amplitude term. This is obtained by matching the observed coherence amplitude to the simple zero extinction 'sinc' model. This stage requires comparison to a 1-D LUT, but unlike the extinction LUT in equation 33, its range is set by the first zero of the sinc function. In this way all observed coherences can be matched to an effective height and no LUT boundary effects occur. Choice of the factor 'ε' weighting the two components is very important and should be chosen to provide robustness to extinction variations. In the zero extinction case it is easy to show that it should be chosen as 0.5, in which case equation 37 gives the exact result for height, regardless of canopy offset structure. In the more general nonzero extinction case ε should be reduced. In the limit of infinite extinction ε tends to zero and the phase centre term tends to the true height. However, practical extinction levels at L band and below are less than 1dB/m (see equation 34). In this case we have found that choice of ε = 0.4 keeps the height error variations with extinction

below 10%. By adopting a constant ε value we then avoid problems of matching extinction to local variations and hence save considerable computation time.

Given its balance between accuracy and ease of computation, we adopt equation 37 as our standard test algorithm for tree height estimation. We now demonstrate its effectiveness by application to POLInSAR test data.

9   POLInSAR Data Processing

In the previous section we covered in some detail the theoretical background to POLInSAR. based vegetation height and ground topography estimation, culminating in a robust and efficient algorithm in equation 37. Here we illustrate and reinforce the ideas introduced by giving an example of a full data processing chain. The data we use is from a 3-D coherent SAR simulator, details of which can be found in [Williams 1999, 2000, 2005,Cloude 2004,2005]. We choose an L band vegetated scene at 45 degrees angle of incidence containing 3 separate layers. The first is a rough dielectric ground, modelled as a tilted Bragg scattering surface. Above this is a short 0.5m vegetation layer modelling understorey. Both these layers cover the whole scene of 100m x 100m. Finally over the central part of the image (56m x 56m) we place a random canopy of branches, similar in structure to a hedge i.e. without major trunk elements. This canopy forms the main source of volume decorrelation in the scene and its regular height of 10m provides a convenient check of the height retrieval accuracy of the various algorithms introduced earlier. The test scenario has the geometry shown in figure 1. Here we see the flat underlying ground with the 10m hedge in the centre of the scene. This layer is comprised of a random Gaussian distribution of branches with mean length of 1.5m and standard deviation of 0.2m with a density or mean volume fraction of 0.2. The L band signal ($\lambda = 0.23061$m) illuminates the scene at $\theta = 45$ degrees incidence from an altitude of 3km, similar to the geometry used by the airborne E-SAR system from DLR in Germany [Papathanassiou 1997]. A 10m horizontal offset baseline is used for the interferometry, again reflecting the typical flight geometry used in repeat pass L band POLInSAR by the ESAR system. The SAR simulator allows convolution of the scattered field with an instrument point spread function, chosen in this case with a resolution of 0.6905m in azimuth and 1.3811m in ground range. The image pixel size is then sampled at 0.5m x 0.5m in ground range and azimuth. These values are typical of those used for airborne sensors.

With these preliminaries we now turn to the processing chain itself:

9.1   Step 1 : Reading POLInSAR Data Files

The first step in POLInSAR is to prepare the appropriate data files. As we need to employ phase information, use is made of single look complex (SLC) data files as opposed to multilook amplitude products. Note also that the well-known Stokes matrix compression scheme as used by JPL-AIRSAR, although useful for polarimetry, is not suitable for POLInSAR studies. As a consequence POLInSAR requires three calibrated (for both radiometry and polarimetry) SLC data files for each spatial position (usually HH, HV and VV). In common with conventional interferometry, the second spatial position (slave track) defining the offset baseline needs to be co-registered with the first (master track). This processing step is common to all polarisation channels and will lead to a small residual loss of coherence due to misalignment errors of the tracks (usually around 1/10 of a pixel accuracy). Such errors (and those associated with signal to noise and quantisation) need in practice to be assimilated into the design of POLInSAR systems. A suggested framework for this has been presented in [Krieger 2005, Cloude 2005]. In practice, the largest error source in POLInSAR has been shown to be temporal decorrelation [Papathanassiou 2003]. In this tutorial however we assume perfect co-registration and ignore such effects. In the simulator perfect co-

registration is possible due to the exact geometry employed and temporal effects can be avoided by maintaining exact scatterer locations between baseline end points.

Hence for a full POLInSAR analysis we require six SLC data files, three from the master and three from the slave. Figure 5 shows a SAR image of the test scene for the 4 channels HH, HV,VH and VV provided by the simulator. Note that for calibrated data HV = VH as required by the reciprocity theorem for backscatter and so only one of the crosspolar channels need be used in the analysis. However providing separate HV and VH data channels can be useful in practice. In the modelling context it can be used to check the co-ordinate system used in the simulator. For forward scattering alignment (FSA) HV and VH will be equal in magnitude but 180 degrees out of phase whereas for the backscatter alignment (BSA) HV = VH in both amplitude and phase. For real SAR data, the HV/VH coherence can also be used as a check of signal to noise ratio in the crosspolar channel. If the HV/VH coherence is high then the SNR is high and vice versa.

In figure 5 we can clearly see the increased backscatter from the hedge layer and note the shadow region at the rear of the hedge due to its 10m elevation. We note too a bright band at the front of the hedge in HH and VV. This is due to a second order ground volume interaction. The simulator accounts for three levels of scattering [Williams 1999, 2000], direct scattering from volume and surface, second order surface-volume interactions and third order surface-volume-surface interactions. While the third order interactions are generally small it is important to model correctly the first and second order interactions, which requires careful calculation of the effective reflection coefficient from the rough surface and also correct modeling of the polarimetric phase for the second order or dihedral component.
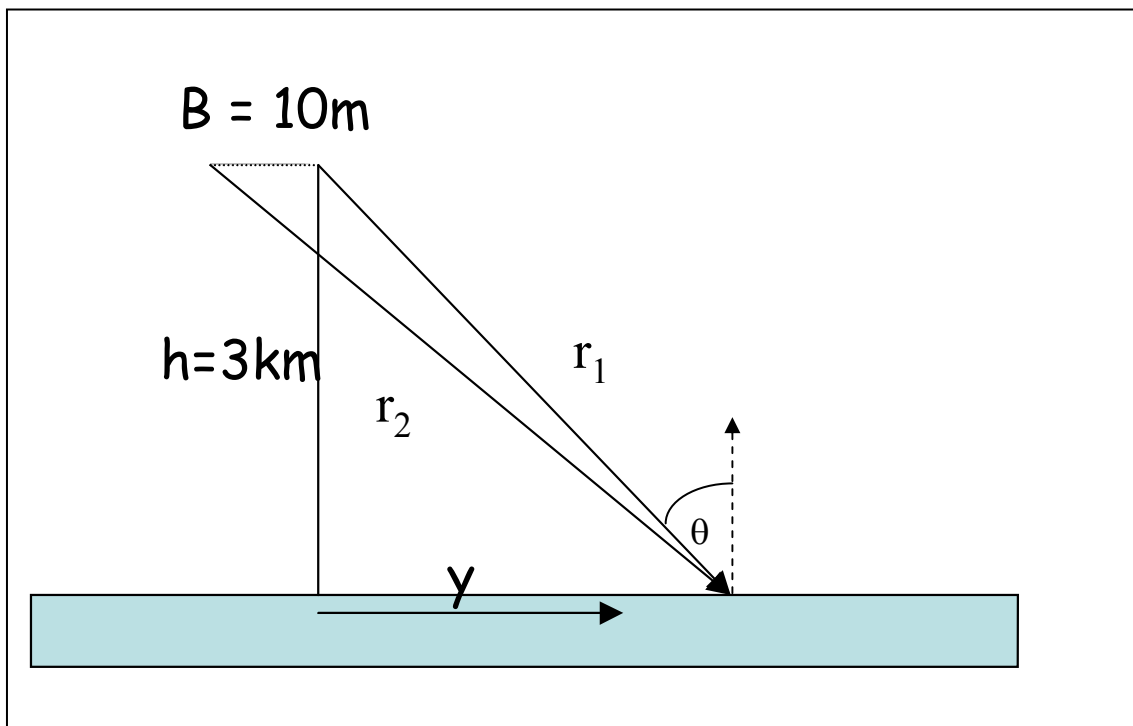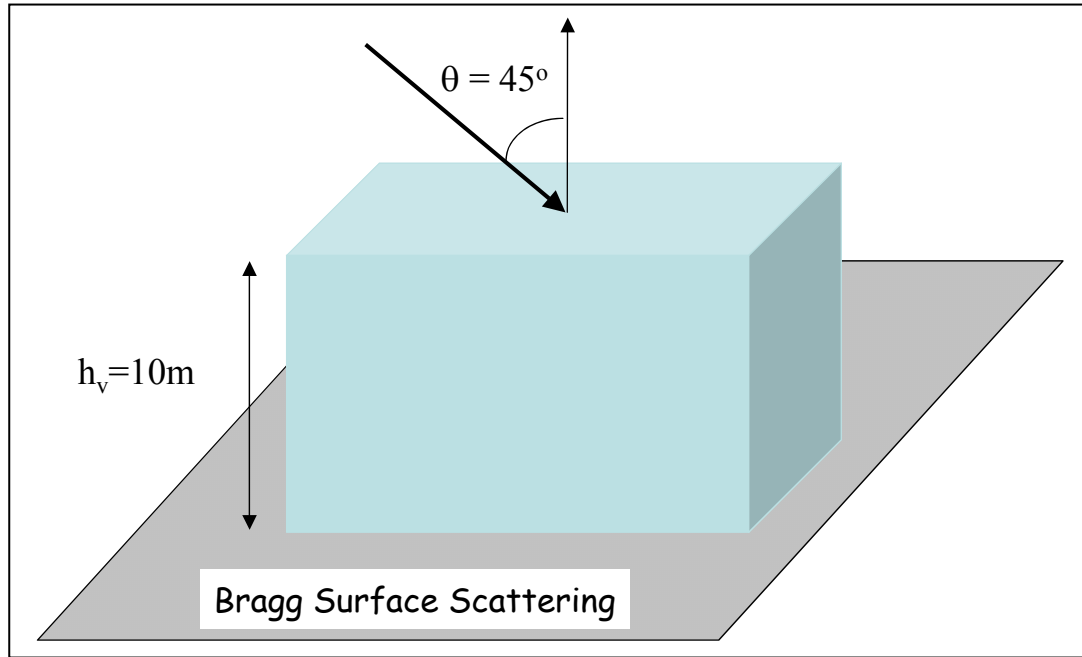
Figure 4 : POLInSAR Simulation Geometry

9.2   STEP 2 : GENERATING AN INTERFEROGRAM

The next step is to generate a complex interferogram $s_1 s_2^*$ using equation 10. For illustration purposes we generate an interferogram for the HV polarization channel. The raw phase of the product is then shown in figure 6. Here we see two features of importance. Firstly we see a background phase variation across the whole scene, which is a function of range only and comprises one complete fringe or 2π phase variation. The second feature we note is the phase noise associated

with the canopy layer. This phase noise is due to volume decorrelation and later we shall use this decorrelation to extract information about the height of the vegetation using POLInSAR.

9.3   STEP 3 : FLAT EARTH REMOVAL

It is possible to remove the background phase variations by employing the geometry of figure 4 to calculate the expected phase variation for a flat surface and then removing this phase by multiplying the interferogram by the complex conjugate of the so called 'flat earth' phase. From the geometry of figure 4, this phase variation can be calculated as

$$e^{i\phi_{fe}} = \exp(i\frac{4\pi}{\lambda}(r_2 - r_1))$$
$$r_1 = \sqrt{h^2 + y^2}$$
$$r_2 = \sqrt{h^2 + (y+B)^2}$$

- 38)

where y is the ground range co-ordinate, which we vary across the scene. When we form the modified interferogram $s_1.s_2^* e^{-i\phi_{fe}}$ we obtain the phase image shown in figure 7. Here we see that the phase of the flat surface is now constant at zero degrees. This becomes our ground phase reference across the whole scene. We can again see the phase noise due to the vegetation layer but note in addition that there is a bias or offset to the mean phase of around 1 radian in this region. This is called vegetation bias and reflects that fact that the mean phase centre in the vegetation lies above the ground (positive phase). Again, in POLInSAR we make use of the variations of this phase centre with polarisation to estimate the vegetation height. Before we can estimate height from phase however we need to calculate the scale factor or vertical wavenumber k_z, which relates phase to height via the relation $\phi = k_z.h$

9.4   STEP 4: VERTICAL WAVENUMBER ESTIMATION

We can calculate the sensitivity of the interferometer to height variations from the geometry of the baseline as follows. [Bamler 1998]

$$\Delta\theta = \tan^{-1}(\tan\theta + \frac{B}{h}) - \theta$$
[1]
$$k_z = \frac{4\pi\Delta\theta}{\lambda\sin\theta}$$

- 39)

We see that this is a function of angle of incidence, for a fixed baseline B, k_z is higher in the near range where θ is small and decreases in the far range when θ increases. However for this small scene of only 100m range swath from 3km altitude the variation of angle of incidence is small and hence k_z is approximately constant with a value of 0.1282 for a 10m baseline. Hence a vegetation bias of 1 radian corresponds to a height of 7.8m. With k_z calculated we can then turn the phase image of figure 7 into an equivalent height map. Figure 8 shows a histogram of the height of the pixels in the canopy zone. Here we see a mean of 5m, half the canopy height, with a significant spread due to the phase noise caused by volume decorrelation.
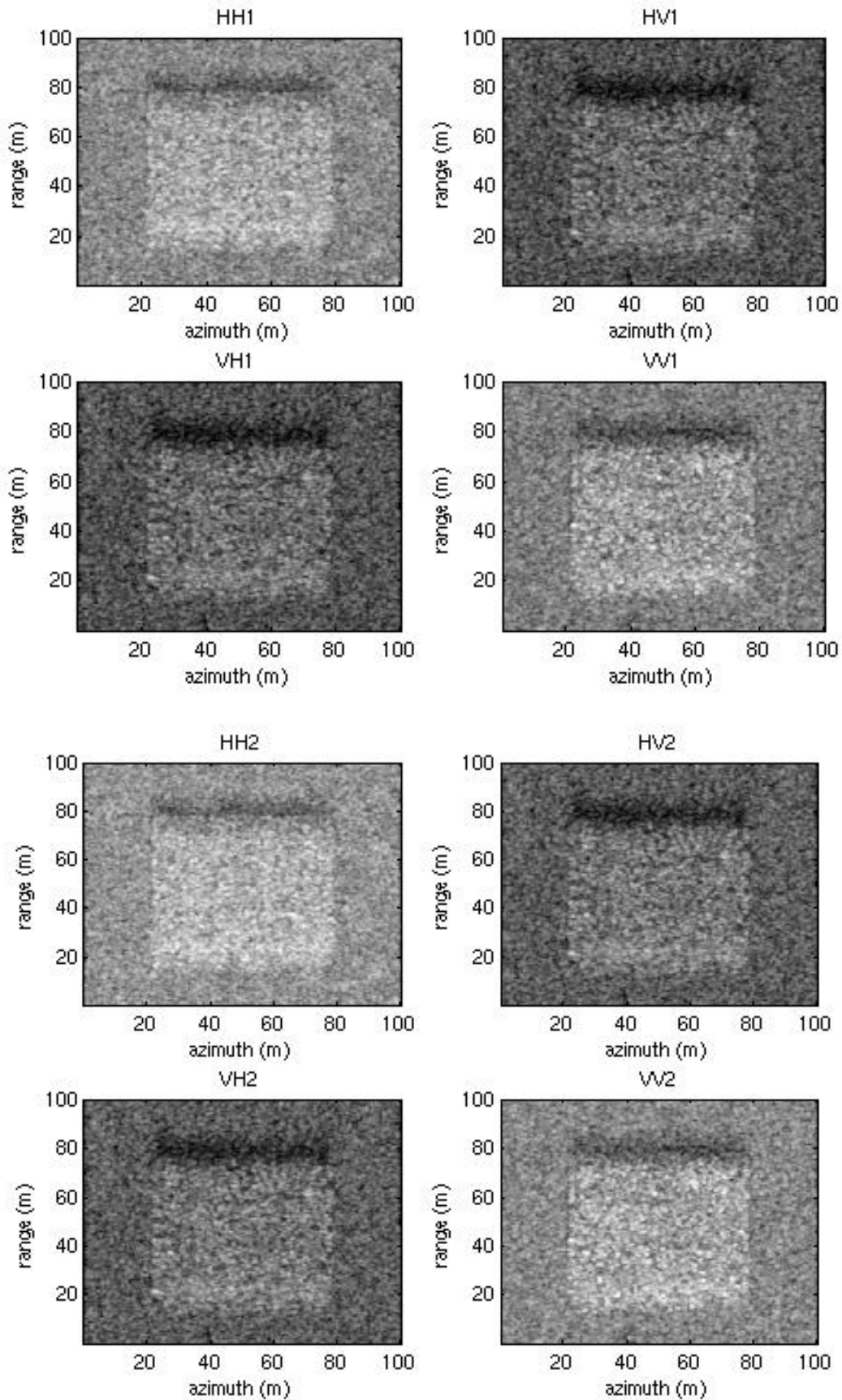
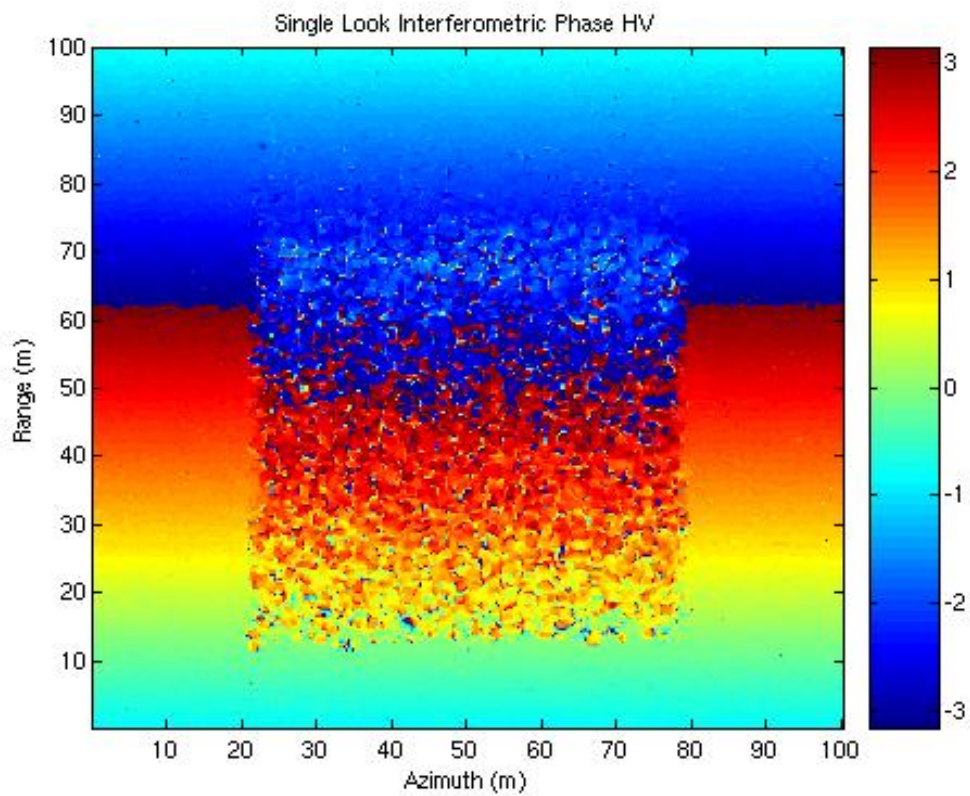*Figure 5 : SAR Images for the 4 polarisation channels and two baseline positions1 and 2 of the simulated scene*

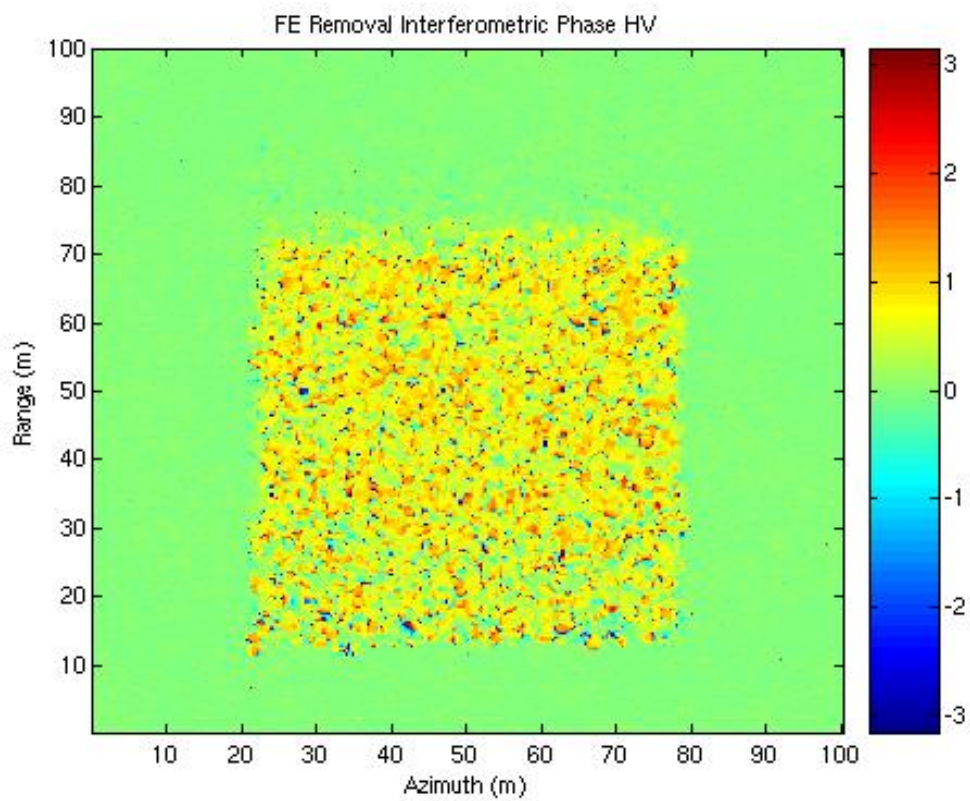*Figure 6 : Raw Phase of the Interferogram for HH Polarisation*

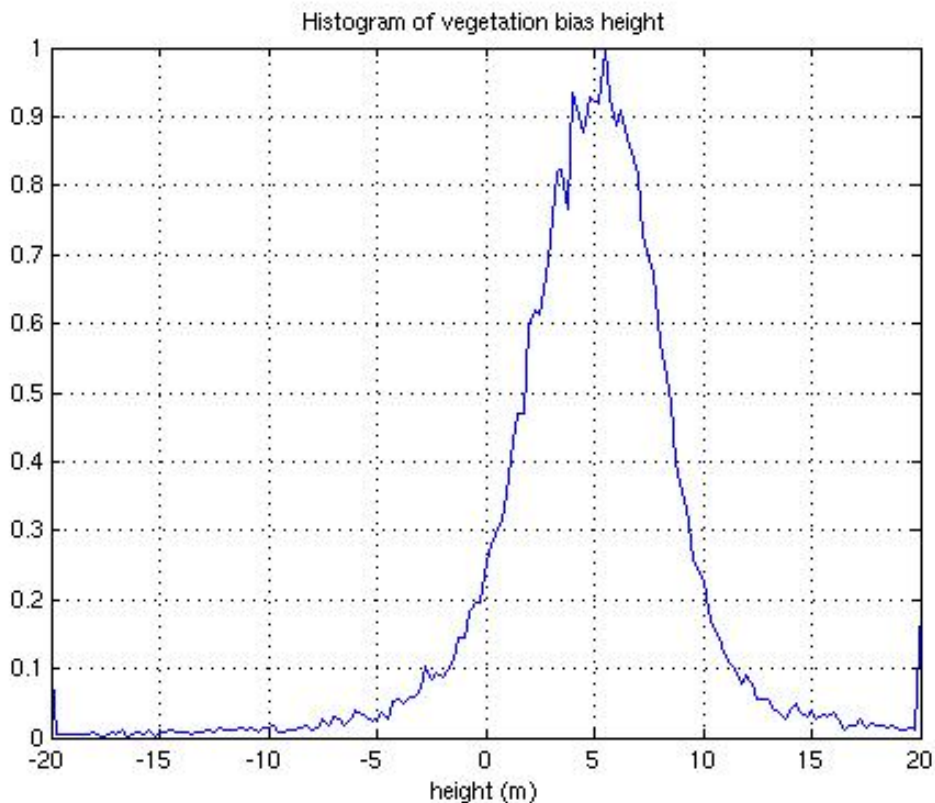*Figure 7 : Interferometric Phase Following Flat Earth Removal*

Figure 8 : Histogram of Phase Centre heights in Canopy Region

We see from this example that the phase of the vegetation bias does not correspond simply to the height itself, but generally underestimates the true height by an amount that depends on extinction, structure and the contribution from surface scattering. Further we don't always know the ground reference phase (in this case zero due to knowledge of the exact geometry) and so in general to estimate height in a robust way we need to take the phase *relative* to some reference point. To do this and further improve the height estimate we first need to include coherence amplitude as well as phase in the inversion.

9.5   STEP 5: COMPLEX COHERENCE ESTIMATION

In order to estimate coherence we employ equation 2, which generates a complex ratio, the phase of which is just the mean phase over the selected pixels and the amplitude of which lies in the range 0 to 1 and relates to the quality of the phase through its local variance. When the summation in the numerator is zero, we have complete decorrelation and a coherence of zero. In this case there is no significant phase information in the selected pixel. At the other extreme when the neighbouring pixels all have the same phase then the coherence is unity and we have a deterministic phase. We can visualise this coherence information in two ways. Firstly we can make an image of the coherence amplitude. This is traditionally viewed as a grey scale image with white = 1 and black = 0 and gives a direct visual interpretation of areas of high and low coherence. However such an image misses completely the important contribution made by phase. To overcome this we employ a mapping of the complex coherence inside a unit circle in the complex plane, with radius equal to the coherence amplitude and phase the polar angle of the coherence point. This circle diagram is shown in figure 9. This has the advantage of displaying both phase and coherence amplitude on the same diagram but is limited to a pixel-by-pixel view rather than an image. Nonetheless it an important

tool in POLInSAR as it allows us to view the variation of both phase and coherence with polarisation and hence check the robustness of inversion algorithms based on the shape of the coherence region, that is the region formed inside the unit circle by changes over the complete set of polarisation combinations.
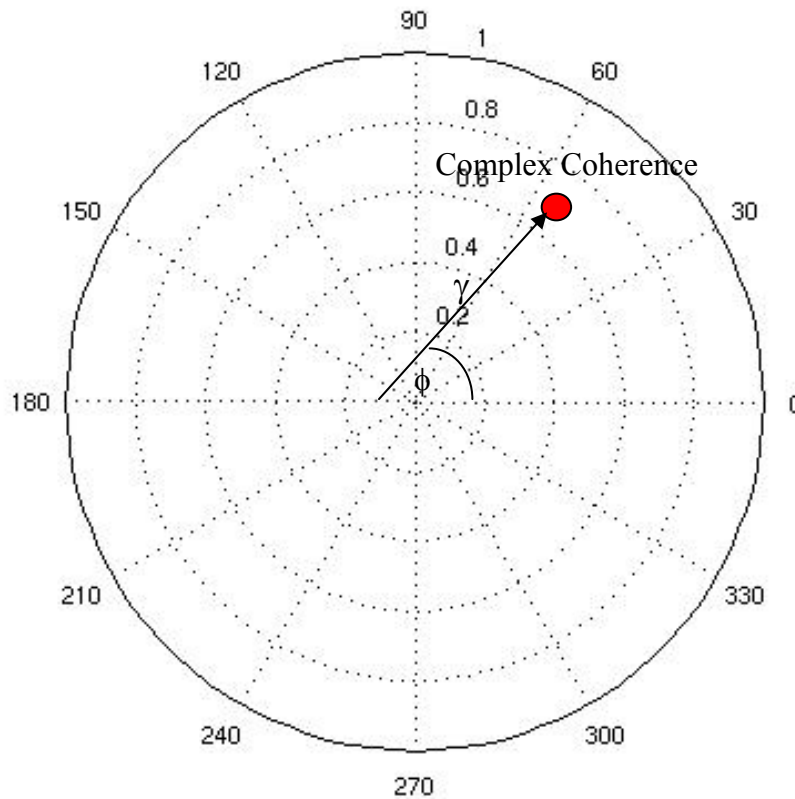

Figure 9: Polar Representation of Complex Coherence inside the unit circle

9.6 STEP 6: COHERENCE BIAS AND CONVERGENCE

To calculate coherence we need to specify a window size for the local averaging process around the pixel under consideration. Coherence is related to phase variance and hence is akin to estimation of second order statistics of a stochastic variable. The choice of window size is therefore crucial to the quality of the estimate of coherence obtained. For example, in the extreme case we might choose a window size of 1x1 and just take the pixel phase itself. In this case all estimated coherences will be unity, but we do not obtain a good estimate of the true value of coherence and have an extreme case of bias in the estimate. As the window size increases we will therefore still obtain a slight overestimation (see figure 1) until for some window size, which depends on the underlying coherence value itself, we obtain convergence to an unbiased estimate with variance limited by the Cramer Rao bounds in equation 9. To illustrate this process, figure 10 shows histograms of the estimated coherence in the canopy region for various window sizes. The window used is square of integer dimension N, where we have used N = 3,7,11, and 15.

Note that the N = 3 window is too small. We see a residual bias in the peak of the histogram and a very wide distribution of coherence points. N = 7 shows some improvement but still a bias offset. N= 11 starts to show some convergence. This we can see because for N = 15 we see little change in the peak of the histogram which occurs around 0.7, although of course there is some narrowing of the width of the distribution for the larger window. For this reason we select N = 11 for further investigations. Figure 11 shows a coherence image of the whole scene for this window

size. Note that the coherence over the surface regions is unity while the coherence over the canopy area reduces due to volume decorrelation. In the phase image we see a smoothed estimate of the vegetation bias already noted in figure 7.
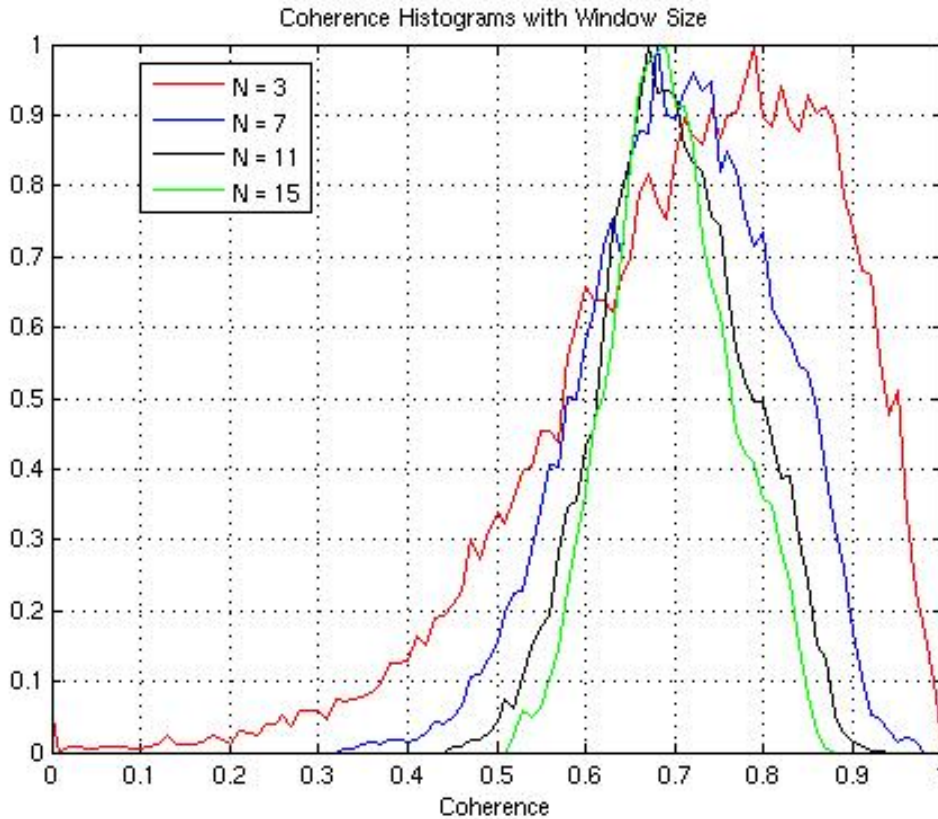

Figure 10 : Histograms of Coherence Estimate versus window size for HV interferogram

Having now established estimates of both phase and coherence we use the data to illustrate the accuracy of three important POLInSAR inversion algorithms. In the first case we take a simple DEM difference between polarisations to try and estimate canopy height. In the second we employ just the coherence amplitude and finally we combine the phase and coherence amplitude together in the algorithm described in equation 37.

9.7 STEP 7: ALGORITHM 1 : DEM DIFFERENCING

In this approach we need to choose 2 polarisation channels, one with a phase centre close to the ground, obtained for polarisation $\underline{w}_s$, and the other with a phase centre close to the canopy top for polarisation $\underline{w}_v$. Differencing the interferograms and normalising by k_z then provides a direct estimate of relative height. There are many ways to choose these two polarisation but here we give a typical example of the logic involved. The cross-polarised or HV channel can often be expected to have a high phase centre, as the ratio of surface to volume scattering is generally small in this case. Hence the 'upper' interferogram can be formed from HV polarisation. To select a lower channel we use the fact that dihedral or double bounce scattering has a phase centre lying on the surface and so as long as the double bounce is stronger than the volume in the selected channel then the phase centre will lie close to the ground. The HH-VV channel is closely matched to such a dihedral component and hence we can choose the second interferogram in this polarisation combination. Figure 12 shows the resulting height estimate.
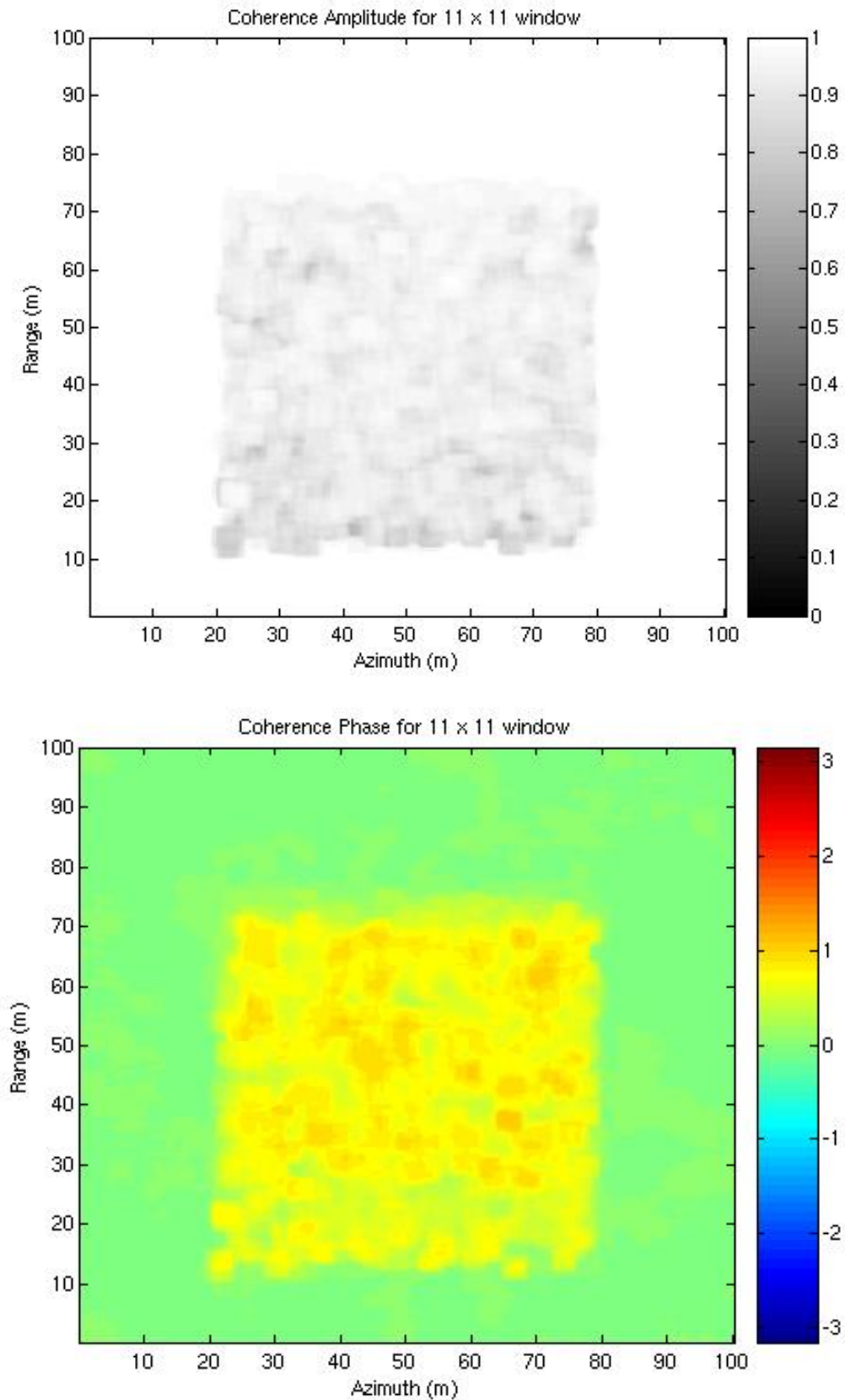
Figure 11: Coherence Image for HV Interferogram using an 11x11 window (amplitude (upper) and phase (lower))
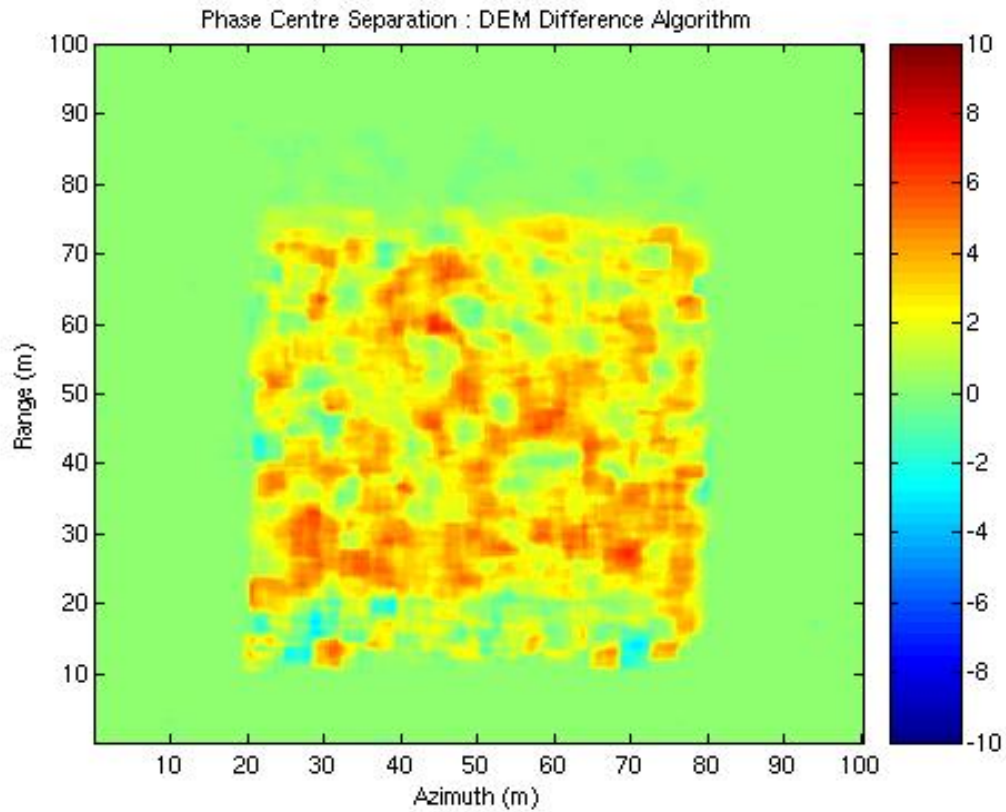
Figure 12 : Height Estimate from Difference of DEMs in HV ands HH-VV channels
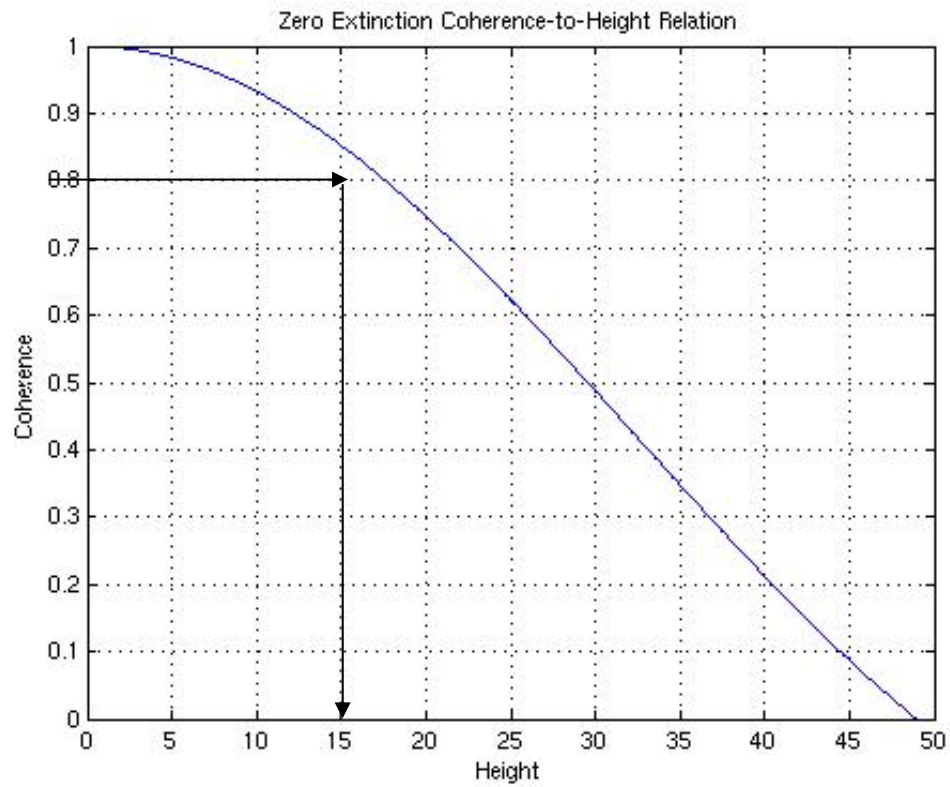

Figure 13 : Height Estimate from Coherence Amplitude

We note two important points:

1. The height is severely underestimated using this algorithm. The phase centres are only separated by a few metres inside the canopy. Physically this is due to the presence of a strong volume scattering component in all polarisation channels and also because the HV phase centre lies not at the top but approximately half way up the volume (see figure 8).

2. The second key point is that sometimes the height estimate is negative. This arises because the HV phase centre lies below the HH-VV and our assumption of the 'upper' and 'lower' phase centres is reversed. This will also have implications for the estimation of ground topography in the full 'rvog' inversion scheme (see figure 15).

9.8   STEP 8: ALGORITHM 2 : COHERENCE AMPLITUDE INVERSION

As an alternative to the DEM differencing approach we can use the coherence amplitude in a channel we believe to have only volume scattering present ($\mu = 0$). Again we can adopt the HV channel as a good approximation to this. We then use the relation between height and coherence for a *known* extinction in the layer. If we assume zero extinction then we obtain the 'sinc' relation shown in figure 13. When we apply this relation to the HV coherence we obtain the height estimates shown in figure 14.
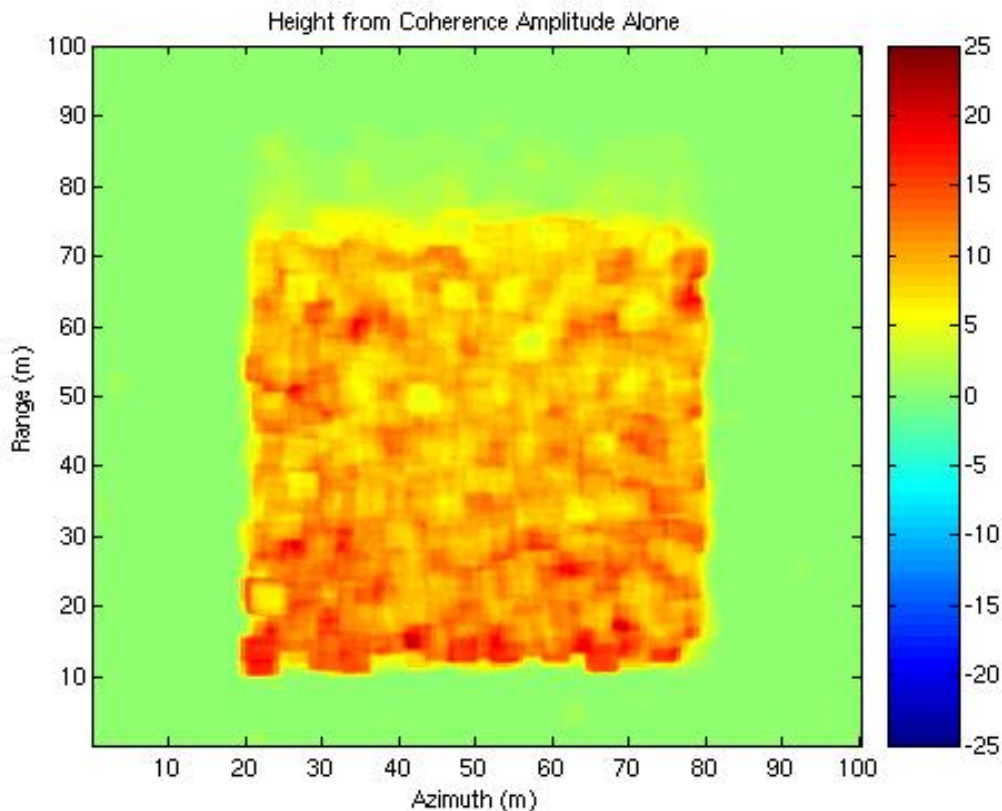

Figure 14 : Height estimate from HV Coherence

Here we see a much better estimate, closer to the true height of 10m. However several points are overestimated and also such an approach is sensitive to density (extinction) and structure (crown depth) variations in the vegetation. For this reason we turn finally to consider the combination of phase and coherence in equation 37 for robust height estimation.

9.9   STEP 9 : GROUND PHASE ESTIMATION USING DUAL POLARISATIONS

The first stage in better using phase information is to try and locate the true ground position. This we can do using just two interferograms in two polarisations, similar to the DEM differencing approach. However this time we employ both the phase and coherence of the two interferograms to compensate the volume offset in the ground channel using equation 30. If we choose HV as the 'volume' dominated channel and HH-VV the 'surface' dominated channel we obtain the ground phase estimate shown in figure15 (again using an 11 x 11 window)
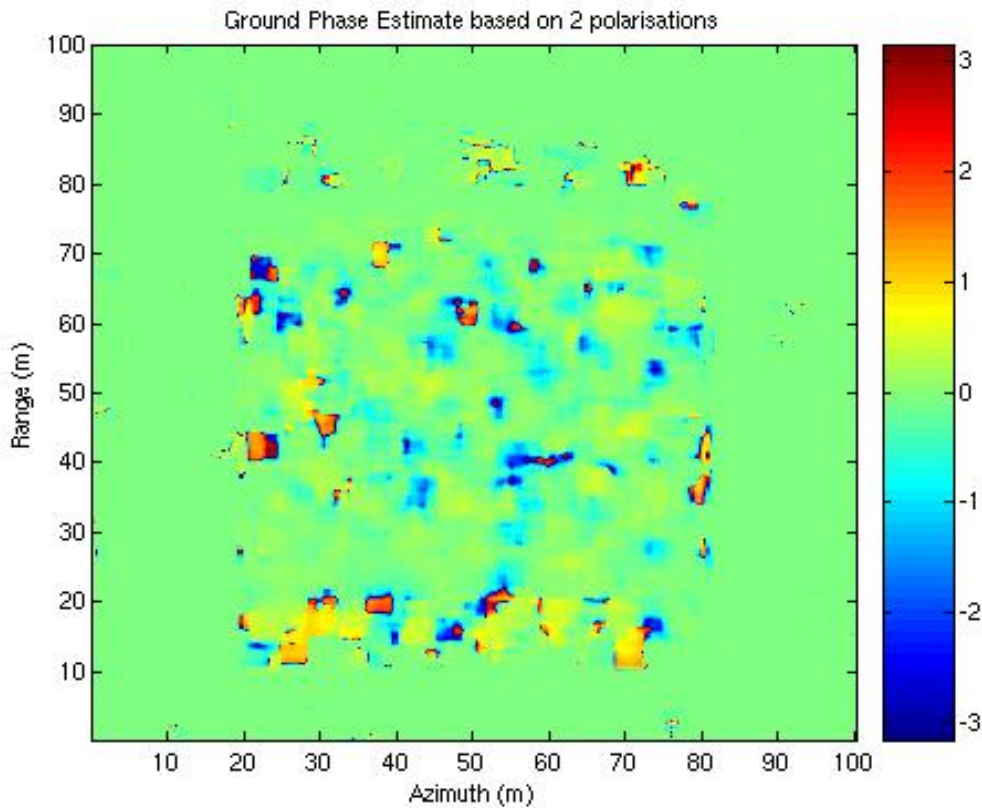

Figure 15 : Ground Phase Estimate Based on HV and HH-VV Interferograms

We note that the true ground phase in this example is zero and can see that most of the vegetation bias has in fact been removed. However, the phase estimate is noisy, due to inversions of the HV and HH-VV phase centres and also to density variations in the canopy. In general therefore ground phase estimation requires a more sophisticated approach than just the simple dual polarisation line fit. In a more sophisticated approach we can use multiple polarisation channels to fit the line parameters in an overdetermined system of equations. In our case however we adopt a simpler solution, namely to filter the phase jumps in figure 15 by using a median filter (note that a conventional smoothing or mean filter would be inappropriate for such phase filtering and the median approach provide a better way to suppress phase jumps of the type observed in figure 15). Figure 16 shows the result of applying a strong 21 x 21 median filter. Here we see some residual phase errors but note that the phase jumps in figure 15 have been removed. Having obtained a better estimate of the true ground position, we can now employ equation 37 to combine phase and coherence information in a way that is robust to structure and density fluctuations.
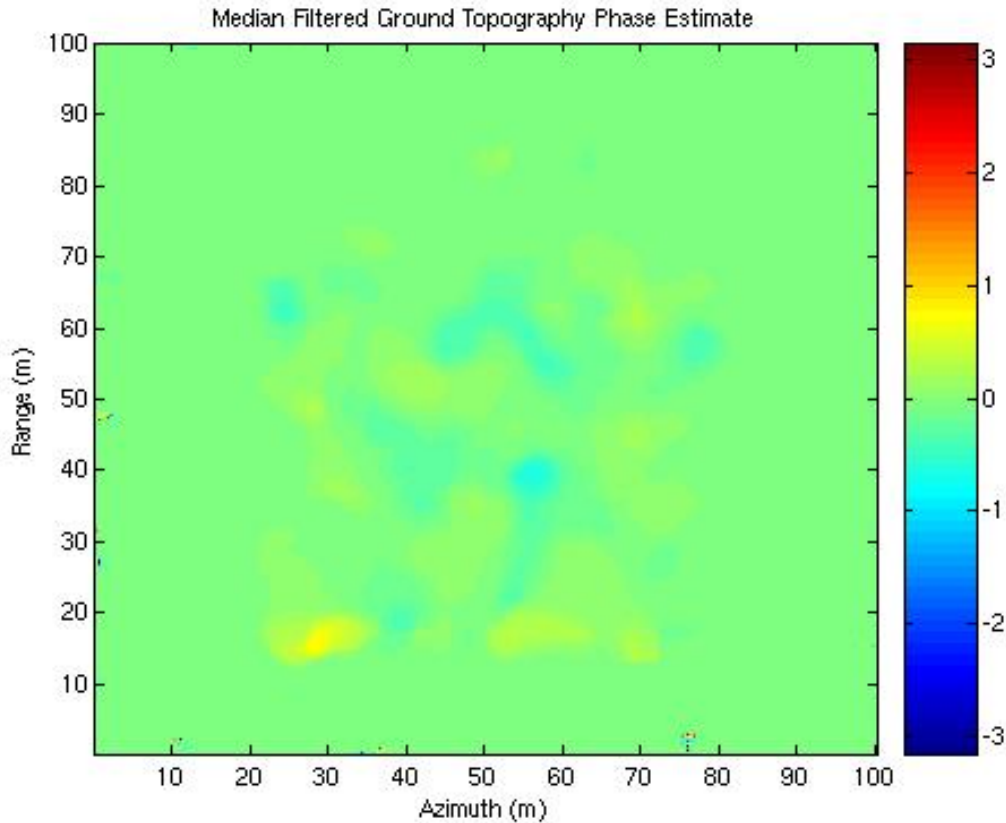
Figure 16: Median Filtered ground Phase Estimate

9.10 STEP 10: ALGORITHM 3: PHASE AND COHERENCE INVERSION

Using figure 16 as an estimate of the ground phase ϕ_o in equation 37, we can then estimate the two components required for height. Firstly we obtain the height of the HV phase centre, now from the estimated ground position, as shown in figure 17. This again confirms a height around half way up the canopy at 5m. The difference between this result and figure 8 is that we are now compensating for arbitrary ground topography variations and hence are providing a more robust algorithm approach. As outlined in the discussion around equation 37, we must now compensate this underestimation of height by adding a fraction of the coherence based height estimate ($\varepsilon = 0.4$). When combined, we obtain the final height image shown in figure 18. Here we see a good estimate of the true 10m height of the canopy. This is confirmed by plotting histograms of the height estimates over the canopy region for the various algorithms as shown in figure 19. Here we confirm that the DEM difference is the poorest method, the coherence amplitude and phase/coherence methods provide similar mean values but the latter has smaller dispersion and, as mentioned earlier, is more robust to vertical structural variations. In figure 20 we show sample azimuth transects through the scene. Here again we see the comparative performance of the various algorithms. Note that the difference between the coherence only and coherence/phase methods may in fact be used to estimate crown occupancy of the volume. In this case the two estimates are similar and so the estimated crown occupancy is 100%, which is correct in this simulation where the canopy components were distributed from ground to top.
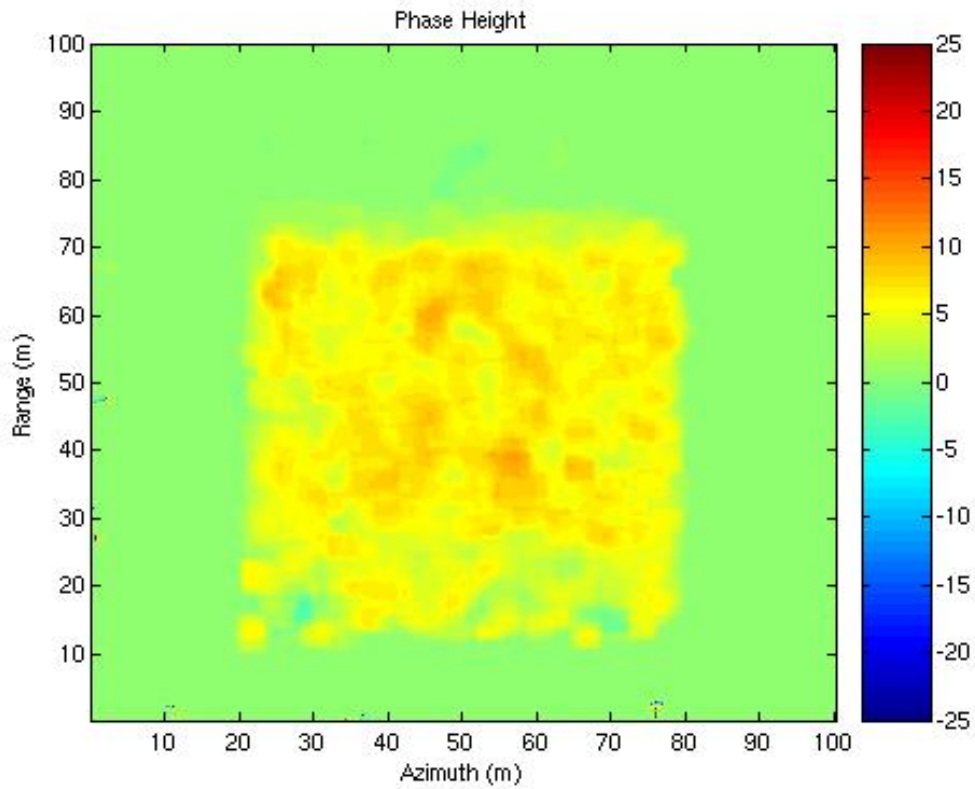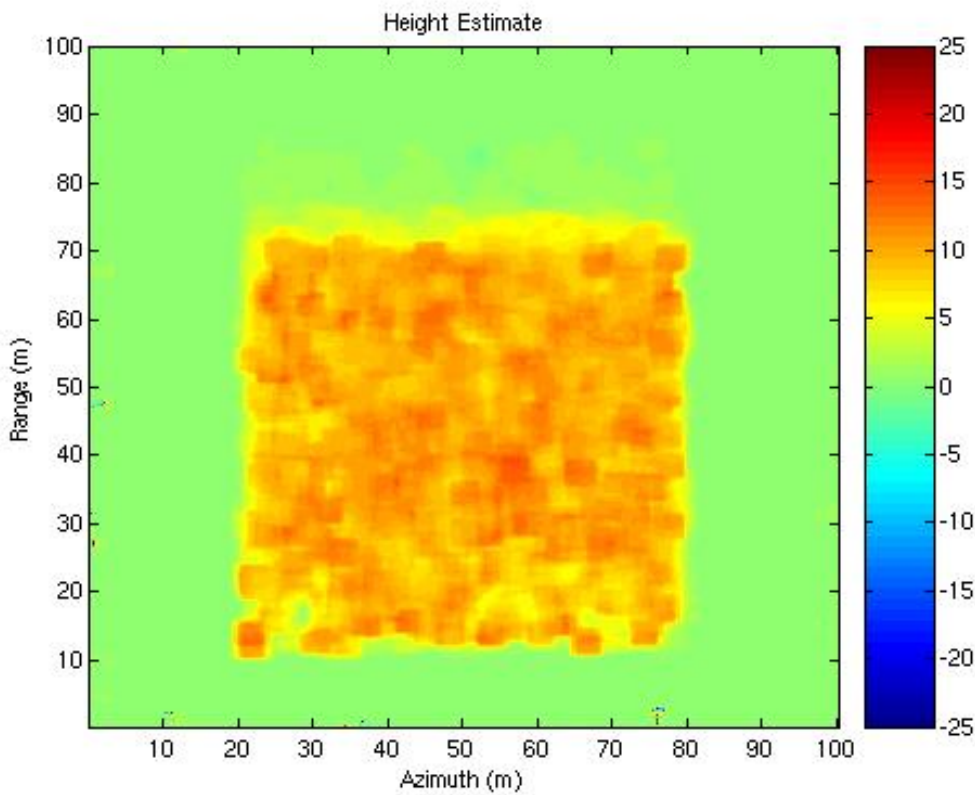
Figure 17: Height Estimate from Ground Phase

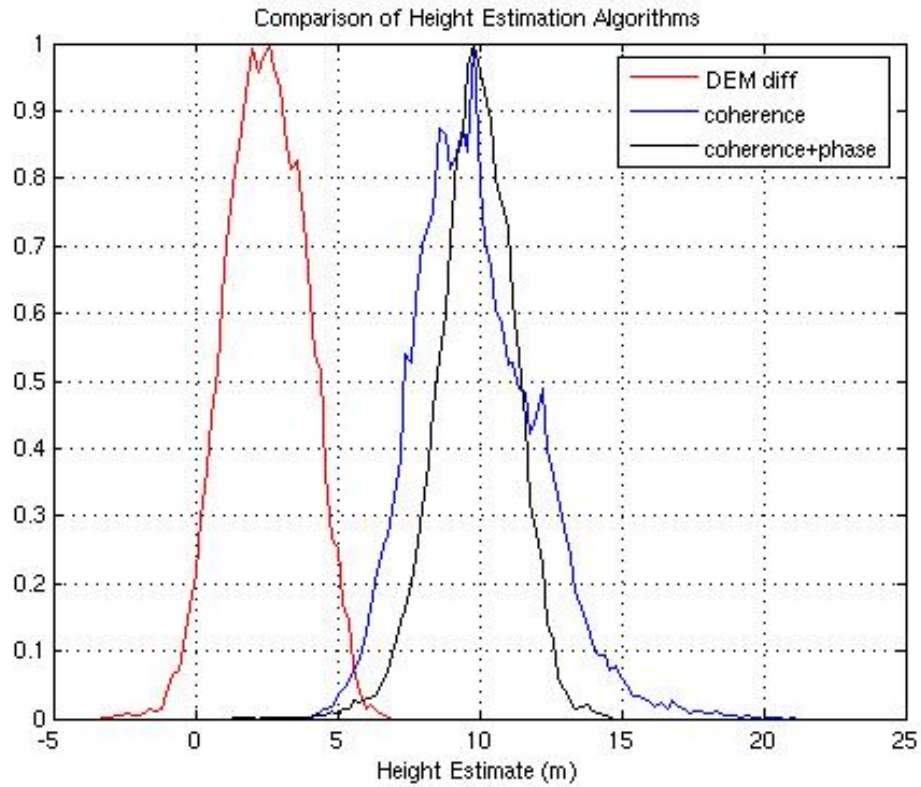*Figure 18: Height Estimate from Combined Phase and Coherence*

Figure 19: Histograms of Height Estimation over Canopy Region for 3 POLInSAR Algorithms
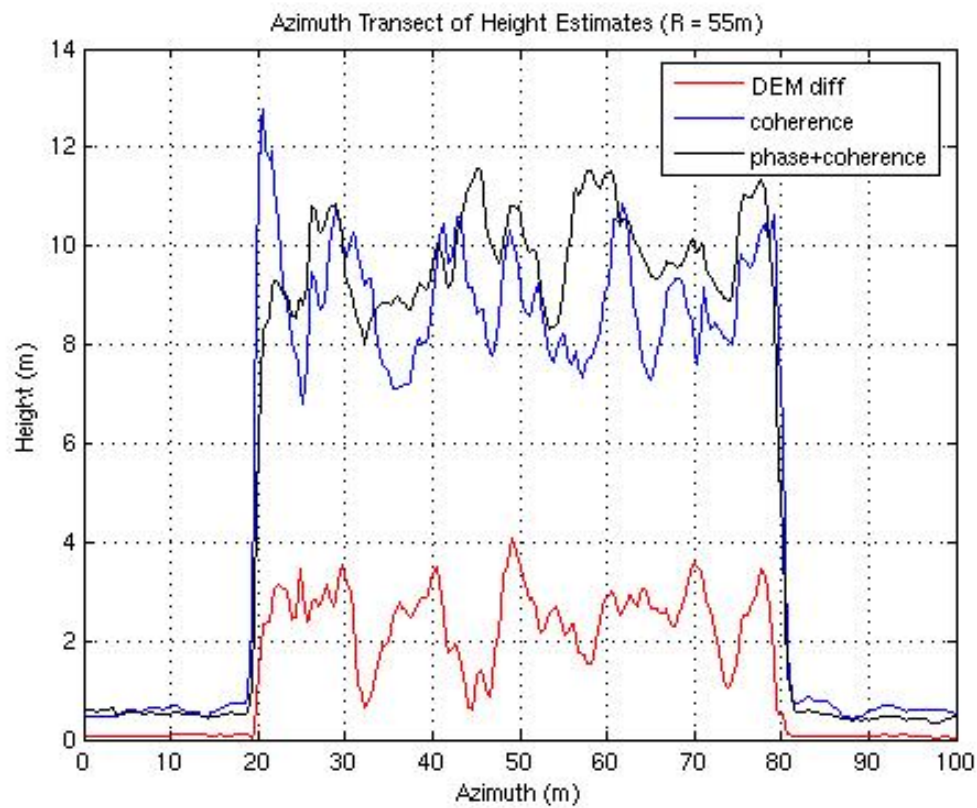

Figure 20: Azmuth Transects through the height profiles for R = 55m (true height = 10m)

9.11 STEP 11: POLARISATION SELECTION

In the previous analysis we have employed just two polarisation channels, HV selected as a volume dominated channel and HH-VV as a surface dominated component. In practice there may be other options available. For example it is common to operate imaging radars in a dual polarisation mode where the transmitter emits a single polarisation but the receiver has 2 orthogonal channels so enabling a co and cross-polar measurement. The JAXA ALOS-PALSAR for example is able to transmit H and receive H and V so obtaining only 2 polarisation combinations HH and HV. It is interesting to see the change in height retrieval performance with this restricted combination. The test data set can be used to investigate this. HV is still used as the volume dominated channel but now we use only HH in place of HH-VV for the surface channel. Figures 21 to 23 show the results obtained.
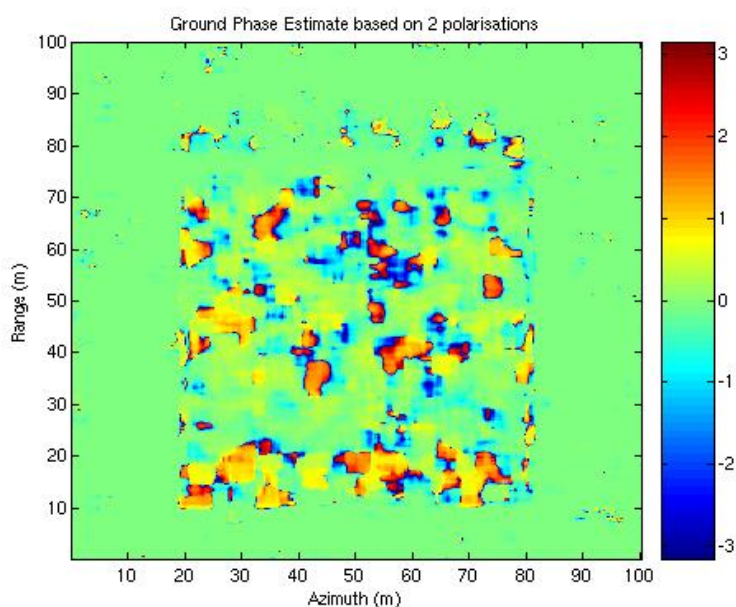

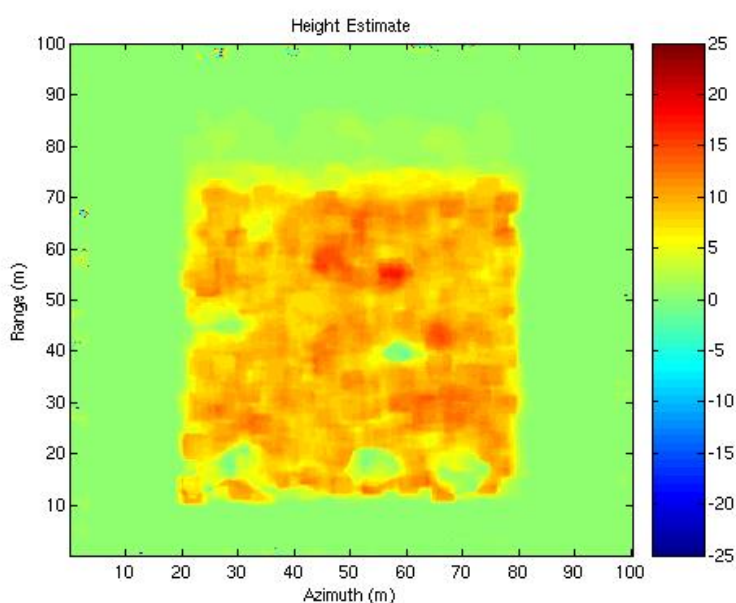*Figure 21 : Ground Phase Estimation using HH and HV channels*

Figure 22 : Height Estimation using Phase+Coherence for HH and HV channels
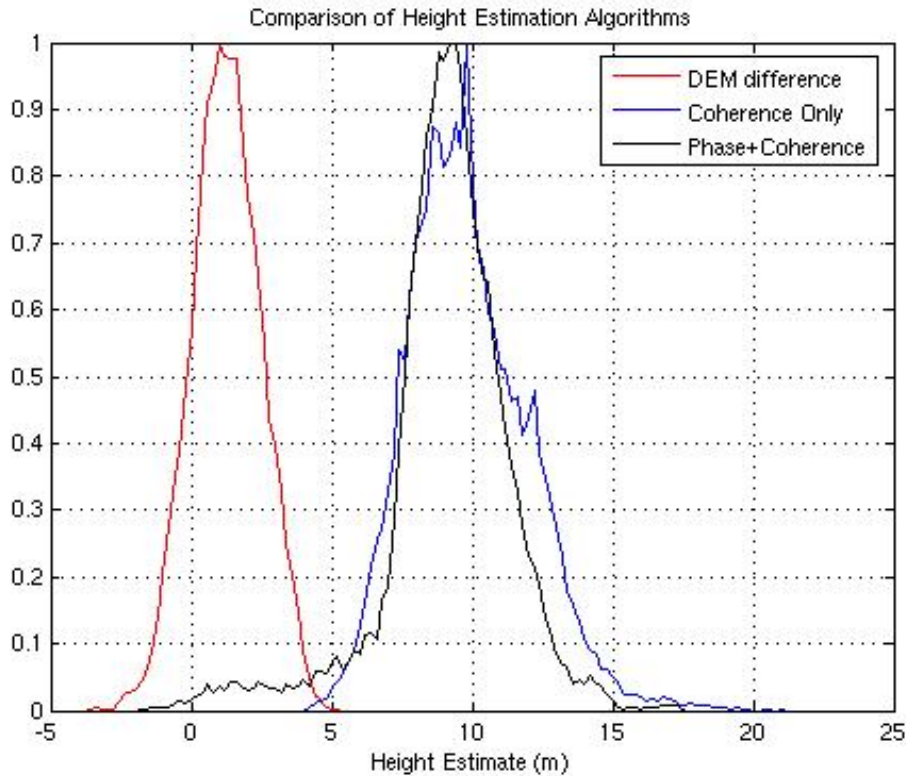
Figure 23 : Histograms of Canopy Height estimation using HH and HV channels

We see some degradation of performance, related primarily to the smaller phase centre separation between the channels. This is particularly noticeable in the ground phase estimation, which is now much noisier. Nonetheless with the same median filtering the height histograms (figure 23) show acceptable performance for mean height estimation.

This was for restricted polarisation switching. At the other extreme, we face the option for Quadpol systems of being able to locally adapt the polarisation vectors $\underline{w}$ to optimise the phase centre separation and hence improve the height estimation further. There are several algorithms being developed to do this and details can be found in the literature [Cloude 1997, Papathanassiou 1999, 2001, Stebler 2002, Gomez Dans 2005] Here we simply illustrate the potential for such adaptive techniques by looking at coherence loci diagrams.

9.12 STEP 12: GENERALISATION TO THE COHERENCE LOCI

In order to investigate the potential for using polarisations other than those listed in table I, we need to calculate the boundary of the coherence region inside the unit circle for all polarisation vectors $\underline{w}$. In general we can allow different $\underline{w}$ vectors at either end of the baseline (equation 16) but to simplify the analysis we follow the suggestion in equations 19 and 20 to use the same polarisation at either end of the baseline. The boundary of the region can then be found using equation 20 [Flynn 2002, Tabb 2001, 2002, Colin 2003]. For each value of phase (equivalent to rotating the unit circle), we obtain the maximum and minimum eigenvalues of the matrix product shown below in equation 40. Having found the eigenvectors corresponding to these eigenvalues we can then use these as $\underline{w}$ vectors to estimate coherence and plot their complex coherences inside the unit circles. By repeating this calculation for all ϕ values we obtain a shape, the boundary of the coherence region. We can then see where our 'standard' polarisations lie within this boundary to assess the potential for using adaptive techniques to improve the inversion.

$$[T]^{-1}[\Omega_H]\underline{w} = \lambda \underline{w} \qquad \begin{cases} [\Omega_H] = \dfrac{1}{2}\left(\Omega_{12}e^{i\phi_1} + \Omega_{12}^{*T}e^{-i\phi_1}\right) \\ [T] = \dfrac{1}{2}\left(T_{11} + T_{22}\right) \end{cases} \qquad \text{- 40)}$$

We use the test data set to illustrate this scheme. Since the coherence regions are plotted inside the unit circle of figure 9 it is a pixel based analysis and so we must select a pixel for analysis. Figure 24 shows a typical example for a pixel location in the canopy region.
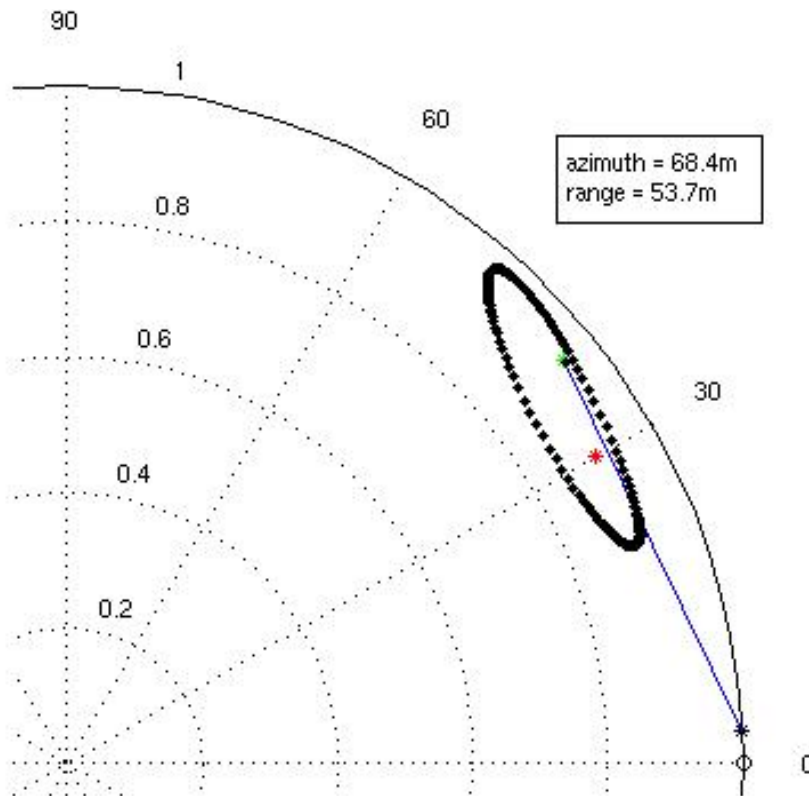

Figure 24 : Coherence region for Pixel in Canopy region (green = HV, red = HH)

Here we show the region boundary in black, calculated using equation 40. In green we show the HV coherence and in blue the HH coherence as used in the height analysis. In blue we show a line between the HV coherence and median filtered topographic phase point. We see that this lies close to the true phase point at zero. We see that in this case optimisation may indeed help the retrieval accuracy. It would be better to use $\underline{w}$ vectors that correspond to the ends of the major axis of the elliptical coherence region. This would maximise the separation of the phase centres and provide a better ground phase estimate. However as the region shape changes from pixel to pixel, this requires an adaptive process that adds considerably to the processing overhead.

10   CONCLUSIONS

In this tutorial we have introduced ina systematic way most of the major concepts required for an understanding of the application of POLInSAR to vegetation parameter estimation. We began by considering the role of coherence in interferometry and polarimetry before exploring in some detail models explaining the variation of coherence with polarisation for surface, volume and the important case of mixed surface and volume scattering. It is in this last case that POLInSAR plays an important role.

We then summarised the main approaches to estimation of vegetation height and ground topography using POLInSAR and developed a fast robust algorithm, based on the random volume over ground or 'rvog' 2-layer coherence model (equation 37). To illustrate these concepts and demonstrate a typical 12 step processing chain we then employed simulated L-band POLInSAR data for a mixed surface and volume scattering scene. We used this to look at issues of coherence and phase estimation before employing the data for a test of various height and ground phase inversion techniques. We concentrated mainly on using dual polarised data but completed the tutorial by looking at the idea of a coherence region and how the polarisation diversity offered by Quadpol systems can be used to further improve performance via the use of adaptive processing techniques.

11   POLInSAR BIBLIOGRAPHY : AUGUST 2005

Askne J, P B Dammert, L M Ulander, G Smith"C-Band Repeat Pass Interferometric SAR Observations of the forest", IEEE Transactions on Geoscience and Remote Sensing, Vol. 35., Jan., pp. 25-35, 1997

Bamler R, P. Hartl, "Synthetic Aperture Radar Interferometry**,** Inverse Problems, 14, R1-R54, 1998

Bessette L A, S Ayasli "Ultra Wide band P-3 and Carabas II Foliage Attenuation and backscatter Analysis", Proceedings of IEEE Radar Conference, 2001, pp 357-362

Cloude S R, E. Pottier, "A Review of Target Decomposition Theorems in Radar Polarimetry", IEEE Transactions on Geoscience and Remote Sensing, Vol. 34 No. 2, pp 498-518, March 1996

Cloude S R, K P Papathanassiou, "Polarimetric Optimisation in Radar Interferometry", Electronics Letters, Vol. 33, N0. 13, June 1997, pp 1176-1178

Cloude S R, K.P. Papathanassiou, "Polarimetric Effects in Repeat-Pass SAR Interferometry", IEEE International Symposium on Geoscience and Remote Sensing (IGARSS '97), Singapore, August 1997

Cloude S R , K P Papathanassiou, "Polarimetric SAR Interferometry", IEEE Transactions on Geoscience and Remote Sensing, Vol 36. No. 5, pp 1551-1565, September 1998

Cloude S R, K P Papathanssiou, A Reigber, "Polarimetric SAR Interferometry at P Band for Vegetation Structure Extraction", Proceedings of 3rd European SAR Conference EUSAR 2000, Munich, Germany, May 2000, pp 249-252

Cloude S R, K P Papathanssiou, W M Boerner "A Fast Method for Vegetation Correction in Topographic Mapping Using Polarimetric Radar Interferometry", Proceedings of 3rd European SAR Conference EUSAR 2000, Munich, Germany, May 2000, pp 261-264

Cloude S R, K P Papathanassiou, W M Boerner, "The Remote Sensing of Oriented Volume Scattering Using Polarimetric Radar Interferometry", Proceedings of International Symposium on Antennas and Propagation, ISAP 2000, Fukuoka, Japan, pp 549-552, August 2000

Cloude S R, I.H. Woodhouse, J. Hope, J.C. Suarez Minguez, P. Osborne, G. Wright, "The Glen Affric Radar Project: Forest Mapping using dual baseline polarimetric radar interferometry", ESA Symposium on "Retrieval of Bio and Geophysical Parameters from SAR for Land Applications", University of Sheffield, England, September 11-14, 2001 pp 333-338

Cloude S R, "Calibration Requirements for Forest Parameter Estimation using POLinSAR", Proceedings of CEOS CalVal Workshop, BNSC Conference Centre, London, September 2002

Cloude, K.P. Papathanassiou, A 3-Stage Inversion Process for Polarimetric SAR Interferometry, Proceedings of European Conference on Synthetic Aperture Radar, EUSAR'02, pp. 279-282, Cologne, Germany, 4-6 June 2002.

Cloude S R, K.P. Papathanassiou, " A 3-Stage Inversion Process for Polarimetric SAR Interferometry", IEE Proceedings, Radar, Sonar and Navigation, Volume 150, Issue 03, June 2003, pp 125-134

Cloude S R, "Radar Polarimetry and Interferometry : A Tutorial Introduction", IEEE Geoscience and Remote Sensing Newsletter, June 2004

Cloude S R, D.G. Corr, M.L. Williams, "Target Detection Beneath Foliage Using Polarimetric SAR Interferometry", Waves in Random Media, volume 14, issue 2, pages S393 - S414., 2004

Cloude S R, M.L.Williams, "The Negative Alpha Filter: A New Processing Technique for Polarimetric SAR Interferometry", IEEE Geoscience and Remote Sensing Letters, Vol. 2, April 2005, pp 187-191

Cloude S R, G Krieger, K Papathanassiou, "A Frammework for Investigating Sp[ace-Borne POLInSAR using the ALOS PALSAR sensor", Proceedings of IEEE Geoscience and Remote Sensing Symposium (IGARSS 2005), Seoul, South Korea, 25-29 July 2005

Colin E., C Titin-Schneider, W Tabbara, "Investigation of Different Interferometric Coherence Optimisation Methods", Proceedings of 1st ESA Workshop on Applications of SAR Polarimetry and Polarimetric Interferometry (POLInSAR 03), January 2003, SP-529, http://earth.esa.int/workshops/polinsar2003/

Colin E., C Titin-Schneider, W Tabbara, " Coherence optimization Methods for Scattering Centre Separation in Polarimetric Interferometry", Journal Of Electromagnetic Waves and Applications (JEWA), in Press, 2005

Dall J, K P Papathanassiou, H Skriver, "Polarimetric SAR Interferometry Applied to Land Ice: First Results", proceedings of IEEE Geoscience and Remote Sensing Symposium (IGARSS '03), Toulouse, France, 2003, Vol III, pp 1432-1434

Flynn T., Tabb M., Carande R., "Coherence region Shape Estimation for Vegetation Parameter Estimation in POLINSAR", Proceedings of IGARSS 2002, Toronto, Canada, pp V 2596-2598

Gatelli F A Monti Guarnieri, F parizzi, P pasquali, C Prati, F Rocca, "The Waveneumber shift in SAR Interferometry", IEEE Trans. GRS-32, pp 855-865, July 1994

Gomez-Dans J.L., S Quegan, "Constraining Coherence Optimisation in Polarimetric Interferometry of Layered Targets", Proceedings of 2nd ESA Workshop on Applications of SAR Polarimetry and Polarimetric Interferometry, POLInSAR 05, January 2005, http://earth.esa.int/workshops/polinsar2005/

Hagberg J O, L Ulander, J Askne"Repeat-Pass SAR Interferometry over Forested Terrain", IEEE Transactions on Geoscience and Remote Sensing, Vol. 33. No. 2, pp. 331-340, 1995

Hajnsek I, S R Cloude, "The Potential of InSAR for Quantitative Surface Parameter Estimation", Canadian Journal of Remote Sensing, Vol. 31, No. 1, pp 85-102, February 2005

Isola M., S.R Cloude, "Forest Height Mapping using Space Borne Polarimetric SAR Interferometry", Proceedings of IEEE International Geoscience and Remote Sensing Symposium (IGARSS 2001), Sydney, Australia, Vol., July 2001

Krieger G., Kostas Papathanassiou, Shane Cloude, Alberto Moreira, Hauke Fiedler, Michael Völker, Spaceborne Polarimetric SAR Interferometry: Performance Analysis and Mission Concepts, Proceedings of 2nd ESA POLInSAR Workshop, Frascati, January 2005, http://earth.esa.int/workshops/polinsar2005/

Lee J S, K W Hoppel, S A Mango, A Miller , "Intensity and Phase Statistics of Multi-Look Polarimetric and Interferometric SAR Imagery", IEEE Trans GE-32, pp. 1017-1028, 1994

Lee J S, M R Grunes, T L Ainsworth, L J Du, D L Schuler, S R Cloude, "Unsupervised Classification using Polarimetric Decomposition and the Complex Wishart Distribution", IEEE Transactions Geoscience and Remote Sensing, Vol 37/1, No. 5, p 2249-2259, September 1999

Lee J S, S.R. Cloude, K.P. Papathanassiou, M.R. Grunes, I. H. Woodhouse, "Speckle Filtering and Coherence Estimation of POLInSAR Data for Forest Applications", IEEE Transactions on Geoscience and Remote Sensing, Vol. 41, No. 10, pp 2254-2263, October 2003

Mette T, K Papathanassiou, I Hajnsek, "Biomass Estimation from POlInSAR over Heterogeneous Terrain", Proceedings of IEEE Geoscience and Remote Sensing Symposium (IGARSS 2004), Anchorage, Alaska, 20-24 September, 2004

Mette T., K Papathanassiou, I Hajnsek, H Pretzsch, P Biber, "Applying a Common Allometric Equation to Convert height from POLInSAR data to Forest Biomass", Proceedings of IEEE Geoscience and Remot Sensing Symposium (IGARSS 2004), Anchorage, Alaska, 2004

Nico G., J M Lopez-Sanchez, J Fortuny,D Tarchi,D leva,A J Sieber, "Assessment of the Impact of Polsarimetric Coherence Optimisation on Phase Unwrapping", Proceedings of 3rd European Conference on Synthetic Aperture Radar (EUSAR 2000), pp 523-526, May 2000

Novak L, M.C. Burl, "Optimal Speckle Reduction in Polarimetric SAR Imagery", IEEE Transactions AES Vol. 26, pp. 293-305, March 1990

Pascual C., E Gimeno-Nieves, J M Lopez-Sanchez, "The Equivalence Between the Polarisation Subspace Method (PSM) and Coherence Optimisation in Polarimetric Radar Interferometry", Proceedings of 4th European Synthetic Aperture Radar Conference, EUSAR 2002, pp 589-592

Papathanassiou K P, A Reigber, R Scheiber, R Horn, A Moreira, S R Cloude"Airborne Polarimetric SAR Interferometry", , Proceedings of IEEE Symposium on Geoscience and Remote Sensing (IGARSS), Seattle, USA, July 6-10, 1998

Papathanassiou K P, A. Reigber, S.R. Cloude "Vegetation and Ground Parameter Estimation using Polarimetric Interferometry Part 1: The Role of Polarisation", Proceedings of ESA CEOS SAR Workshop, Toulouse, France, October 1999.

Papathanassiou K P, A. Reigber, S.R. Cloude "Vegetation and Ground Parameter Estimation using Polarimetric Interferometry Part 2 : Parameter Inversion and Optimal Polarisations", Proceedings of ESA CEOS SAR Workshop, Toulouse, France, October 1999.

Papathanassiou K P, S R Cloude, A Reigber, "Single and Multi-Baseline Polarimetric SAR Interferometry over Forested Terrain", Proceedings of 3rd European SAR Conference EUSAR 2000, Munich, Germany, May 2000, pp 123-126

Papathanassiou K P, S.R. Cloude, "Single Baseline Polarimetric SAR Interferometry", IEEE Transactions Geoscience and Remote Sensing, Vol 39/11, pp 2352-2363, November 2001

Papathanassiou K P, S R Cloude, "The Effect of Temporal Decorrelation on the Inversion of Forest Parameters from POlInSAR Data"", Proceedings of IEEE International Geoscience and Remote Sensing Symposium (IGARSS 2003), Toulouse, France, July 21-25, 2003

Papathanassiou K P, S.R. Cloude , A Liseno, T. Mette , and H. Pretzsch, "Forest Height Estimation by means of Polarimetric SAR Interferometry: Actual Status and Perspectives", Proceedings of 2nd ESA POLInSAR Workshop, Frascati, Italy, January 2005,
http://earth.esa.int/workshops/polinsar2005/

Papathanassiou K P, I. Hajnsek , Thomas Nagler , and Helmut Rott "Polarimetric SAR Interferometry for Snow Cover Parameter Estimation", Proceedings of 2nd ESA Workshop on Applications of SAR Polarimetry and Polarimetric Interferometry, POLInSAR 05, January 2005,
http://earth.esa.int/workshops/polinsar2005/

Pottier E., L Ferro-Famil, S Cloude, I Hajnsek, K Papathanassiou, A Moreira, T Pearson, Y Desnos, "PolSARpro v2.0: The Polarimetric SAR Data Processing and Educational Toolbox", Proceedings of IEEE Geoscience and Remote Sensing Symposium (IGARSS 2005), Seoul, South Korea, 25-29 July 2005

Preiss M, N J Stacy, "Scene Coherence at X-Band from Repeat Pass Polarimetric Interferometry", Proceedings of IEEE Geoscience and Remote Sensing Symposium (IGARSS 2005), Seoul, South Korea, 25-29 July 2005

Reigber A, K P Papathanassiou, S R Cloude, A Moreira, "SAR Tomography and Interferometry for the Remote Sensing of Forested Terrain", Proceedings of 3rd European SAR Conference EUSAR 2000, Munich, Germany, May 2000, pp 137-140

Sagues L, J M Lopez-Sanchez, J Fortuny, X Fabregas, A Broquetas, A J Sieber, "Indoor experiments on Polarimetric SAR Interferometry**", IEEE GRS-38, pp 671-684, March 2000

Sagues L, J M lopez-Sanchez, J Fortuny, X Fabregas, A Broquestas, A J Sieber, "Polarimetric Radar Interferometry for improved Mine Detection and Surface Clutter Rejection", IEEE GRS-39, pp 1271-1278, June 2001

Schneider R Z, K P Papathanassiou, I hajnsek, A Moreira, "Polarimetric Interferometry over Urban Areas: Information Extraction using Coherence Scatterers", Proceedings of IEEE International Geoscience and Remote Sensing Symposium (IGARSS 2005),Seoul, Korea, 25-29 July 2005

Seymour S., Cumming I.G., "Maximum Likelihood Estimation for SAR Interferometry", Proceedings of IEEE-IGARSS'94, Pasadena, USA

Stebler, O., Meier, E., Nueesch, D., "Multi-baseline polarimetric SAR interferometry - first experimental spaceborne and airborne results". ISPRS Journal of Photogrammetry and Remote Sensing, 56(3), 2002

Tabb M, R Carande, "Robust Inversion of Vegetation Structure Parameters from Low Frequency Polarimetric Interferometric SAR"Proceedings of IEEE International Geoscience and Remote Sensing Symposium (IGARSS 2001), Sydney, Australia, Vol., pp , July 2001

Tabb M., Flynn T., Carande R., "Direct Estimation of Vegetation Parameters from Covariance Data in POLINSAR", Proceedings of IGARSS 2002, Toronto, Canada, pp III 1908-1910

Tabb M., J Orrey, T Flynn, R Carande, "Phase Diversity: A Decomposition for Vegetation Parameter Estimation using Polarimetric SAR Interferometry", Proceedings of 4th European Synthetic Aperture Radar Conference, EUSAR 2002, pp 721-724

Touzi R, A Lopes, J Bruniquel, P W Vachon, "Coherence Estimation for SAR Imagery**", IEEE Transactions Geoscience and Remote Sensing, Vol. 37/1, pp 135-149, January 1999

Treuhaft R N, S. Madsen, M. Moghaddam, J.J. van Zyl, "Vegetation Characteristics and Underlying Topography from Interferometric Data", Radio Science, Vol. 31, Dec, pp. 1449-1495, 1996

Treuhaft R N, S R Cloude, "The Structure of Oriented Vegetation from Polarimetric Interferometry", IEEE Transactions Geoscience and Remote Sensing, Vol 37/2, No. 5, p 2620, September 1999

Treuhaft R N, P. Siqueria, "Vertical Structure of Vegetated Land Surfaces from Interferometric and Polarimetric Radar", Radio Science, Vol. 35(1), pp 141-177, January 2000

Williams M.L., "Prediction and Observation of SAR Clutter from Vegetation Canopies", Proceedings of IGARSS '99, Hamburg, Germany, pp 1983-1985

Williams M. L.,"Simulating Low Frequency SAR Clutter from a Pine Forest", Proeedings of 3rd European SAR Conference (EUSAR), 23-25 May, 2000, Munich, Germany, pp 149-152

Williams, M L S R Cloude, 'Predictions of SAR Polarimetry and InSAR Coherence for a Model Wheat Canopy", Proceedings of IEEE Geoscience and Remote Sensing Symposium (IGARSS 2005), Seoul, South Korea, 25-29 July 2005

Yamada H, Y Yamaguchi, E Rodriguez, Y Kim, W M Boerner,"Polarimetric SAR Interferometry for Forest Canopy Analysis by Using the Super-resolution Method"
IEICE Transactions on Electronics, VOL.E84-C, No.12, 2001, pp1917-1924, December 2001

Zebker H A, J Villasenor, "Decorrelation in Interferometric Radar Echoes", IEEE Transactions on Geoscience and Remote Sensing, Vol. 30. No. 5, pp. 950-959, September 1992